Numerical Investigation of Turbulent Combustion Regimes on Localized Forced Ignition using Stratified Combustible Mixture

by

Hitha Lokanath Uchil

A Thesis submitted in Partial Fulfillment of the

Requirements for the degree of

Master of Applied Science

in

Mechanical Engineering

Faculty of Engineering and Applied Science

University of Ontario Institute of Technology

Oshawa, Ontario, Canada

March, 2019

THESIS EXAMINATION INFORMATION

Submitted by: Hitha Lokanath Uchil

Master of Applied Science in Mechanical Engineering

Thesis title: Numerical Investigation of Turbulent Combustion Regimes on Localized Forced Ignition using Stratified Combustible Mixture

An oral defense of this thesis took place on April 17, 2019 in front of the following examining committee:

Examining Committee:

Chair of Examining Committee	Dr. Martin Agelin-Chaab
Research Supervisor	Dr. Dipal Patel
Examining Committee Member	Dr. Xianke Lin
External Examiner	Dr. Bale Reddy

The above committee determined that the thesis is acceptable in form and content and that a satisfactory knowledge of the field covered by the thesis was demonstrated by the candidate during an oral examination. A signed copy of the Certificate of Approval is available from the School of Graduate and Postdoctoral Studies.

Abstract

Localized forced ignition of turbulent stratified mixtures has been numerically analyzed based on three- dimensional Direct Numerical Simulations (DNS) for different values of Karlovitz number (Ka) corresponding to different turbulent combustion regimes. The initial values of turbulent fluctuations $\left(\frac{u'}{S_{b(\phi=1)}}\right)$ and the integral length scale $\left(\frac{L_{11}}{l_f}\right)$ of turbulence have been modified to bring about the change in Ka. The localized forced ignition is accounted by a source term in the energy transport equation which deposits energy over a time interval. It has been found that combustion takes place predominantly under a premixed mode of combustion following successful ignition. An increase in Ka has shown an increase in Minimum Ignition Energy (MIE) and has been shown to have adverse effects on the burned gas mass. Additionally, a stratified combustion mixture has been found to be a more favorable choice over homogeneous mixtures for a given turbulent flow condition for achieving a higher burning rate.

Keywords: Stratified mixture; direct numerical simulation; localized forced ignition; equivalence ratio; karlovitz number; minimum ignition energy

Author's Declaration

I hereby declare that this thesis consists of original work of which I have authored. This is a true copy of the thesis, including any required final revisions, as accepted by my examiners.

I authorize the University Of Ontario Institute Of Technology to lend this thesis to other institutions or individuals for the purpose of scholarly research. I further authorize University of Ontario Institute of Technology to reproduce this thesis by photocopying or by other means, in total or in part, at the request of other institutions or individuals for the purpose of scholarly research. I understand that my thesis will be made electronically available to the public.

Hitha Lokanath Uchil

Statement of Contributions

Part of the work has been published in the Conferences as:

- H.Uchil, D.Patel, "Effects of Karlovitz number on Localized Ignition of Turbulent Combustible Mixture: A DNS Study", *in Proceedings of Combustion Institute - Canadian Section Spring Technical Meeting Ryerson University, Toronto, Canada, May 14-17, 2018.*

- K.Modi, H.Uchil, D.Patel, "Effects of Combustion Regimes on Localized Forced Ignition of Turbulent Stratified Mixture", *in Proceedings of the* 4^{th} *World-Congress on Momentum, Heat and Mass Transfer (MHMT'19) Rome, Italy, April 10-12, 2019* .

Dedication

To my beloved parents & family for their love, endless support, encouragement & sacrifices and to the loving memory of my grandmother *Krishnaveni Giridhar Uchil* (August 14, 1941 - August 23, 2016).

Acknowledgments

This work was carried out at the Faculty of Engineering and Applied Science, University of Ontario Institute of Technology, Canada.

First of all I would like to thank my supervisor Dr. Dipal Patel for providing me an opportunity to complete my master's thesis. I am grateful for his patient guidance, encouragement and advice he has provided throughout my research study and above all for providing opportunities for conferences. Thank you for all those valuable discussions and for deep insights that helped me at various stages of my research. I want to thank him not only for the financial support but also for the concern and support throughout the course of my Master's program.

A special acknowledgment for Compute Canada for computational support and a heartfelt thanks to all my supportive wonderful friends. I also thank all the departmental staff for helping me during the time of my study both academically and officially.

Finally, but most certainly not least, I would like to thank my parents, Lokanath Uchil and Nayana Uchil and my dear sister, Deepta Uchil for their unconditional love, encouragement and support and without which I would not have come this far.

Contents

List of Figures

List of Tables

Nomenclature

Roman Symbols

A_q	Constant in the Gaussian distribution equation
a_{sp}	Parameter that determined the total energy deposited by the igniter
B	Pre-exponential factor
b_{sp}	Energy duration parameter
c	Reaction progress variable
C_P	Specific heat capacity at constant pressure
C_V	Specific heat capacity at constant volume
D_{th}	Thermal diffusivity
D_t	Eddy thermal diffusivity
E	Stagnation internal energy
E_{ac}	Activation energy
F	Flammability factor
h_α	Enthalpy of the formation of the species α
H_ϕ	Heat release per unit mass of fuel
Ka	Karlovitz number
L	Computational domain length
l_f	Zel'dovich flame thickness
L_{11}	Longitudinal integral length scale
l_ϕ	Length scale of mixture inhomogeneity
M_b	Normalized burned gas mass
m_b	Burned gas mass
N	Number of species
N_g	Number of grid points

N_ξ	Scalar dissipation rate of the mixture fraction
P	Pressure
Pr	Prandtl number
R	Width of the Gaussian profile
r	Radial distance from the centre of the igniter
R_0	Universal gas constant
Re	Reynolds number
Re_t	Turbulent reynolds number
Re_λ	Reynolds number based on Taylor micro scale
s	Mass of the oxidizer consumed per unit mass of fuel consumption
$S_{b(\phi)}$	Laminar burning velocity at equivalence ratio ϕ
S_L	Unstrained laminar burning velocity of the stoichiometric mixture
Sc	Schmidt number
T_0	Initial temperature
T_C	Critical temperature
t_f	Flame chemical time scale
T_P	Temperature of the products
T_R	Temperature of the reactants
T_η	Life time for the small eddies of turbulence
T_{ad}	Adiabatic flame temperature
T_{ref}	Reference temperature
t_{sp}	Time duration over which energy is deposited by the igniter
u_i	i^{th} component of the velocity vector
Y_F	Fuel mass fraction
Y_O	Oxidizer mass fraction
Y_α	Mass fraction of the species α
$Y_{F\infty}$	Fuel mass fraction in the pure fuel stream

$Y_{Fb(\phi)}$	Fuel mass fraction in the burned gas corresponding to ϕ
$Y_{Fu(\phi)}$	Fuel mass fraction in the unburned gas corresponding to ϕ
$Y_{O\infty}$	Oxidizer mass fraction in air

Accents

$\bar{\rho}$	Mean density
$\dot{\omega_F}$	Normalised fuel reaction rate magnitude
$\dot{Q}$	Ignition power
$\dot{w_c}$	Reaction progress variable reaction rate
$\dot{w_T}$	Source term origination from heat release due to combustion
$\dot{w_\alpha}$	Chemical reaction rate
$\hat{T}$	Instantaneous temperature
B^*	Pre-exponential factor related constant
u'	RMS of turbulent velocity
ϕ'	RMS of equivalence ratio
ξ'	RMS of mixture fraction driven by ϕ fluctuations

Abbreviations

3D	Three-Dimensional
CFD	Computational Fluid Dynamics
DI	Direct Injection
DNS	Direct Numerical Simulations
GDI	Gasoline Direct Injection
IC	Internal Combustion
MIE	Minimum Ignition Energy
PDF	Probability Density Function
RMS	Root Mean Square
SI	Spark Ignition

Symbols

α_i	Thermal conductivity of given species i
β	Zel'dovich number
$\triangle x$	Grid spacing
δ_{th}	Thermal flame thickness
η	Kolmogorov length scale
γ	Ratio of specific heats
λ	Taylor micro scale
μ	Dynamic viscosity
ν	Kinematic viscosity
ϕ	Equivalence ratio
ρ	Density
τ	Heat release parameter
τ_{ij}	Viscous stress tensor
ε	Dissipation rate
ξ	Mixture fraction
ξ_{lean}	Lean flammability limit
ξ_{rich}	Rich flammability limit
ξ_{st}	Stoichiometric mixture fraction

Chapter 1

Introduction

This chapter constitutes the primer part of the thesis topic. Combustion and different ignition sources are defined from imperative point of view. Furthermore, computational analysis, taken under for the apprehended thesis is also been discussed.

1.1 Combustion

In recent times, the world has been confronted with an energy crisis due to depletion of resources and increased environmental problems [53]. The situation has led to the search for fuel, which should be not only sustainable but also environment friendly. Combustion has many impacts on aspects of lives, on sustainability, global climate change and utilization of energy. Improving the design for safer, efficient and non-polluting combustion systems for many different fuels is a challenge for many engineers [53]. The field of combustion is an extremely multi-discipline area, covering thermodynamics, fluid mechanics, chemical kinetics, and many more.

Today, nearly all combustion system must satisfy governmentally imposed stringent emission standards for combustion products, such as carbon monoxide, hydrocarbons, nitrogen oxides, sulphur dioxide and particulate emissions. The emission standards are set at sufficiently low levels to keep the ambient air clean enough to protect the surrounding. Low emissions are achieved by a combination of fuel se-

lection and preparation, combustion system design and treatment of products from combustion [34, 61].

Combustion can be further classified by (1) the reactant mixture, that is homogeneous or heterogeneous, (2) depending on if the oxidizer and the fuel are premixed, or meet only at a point of reaction, and on (3) the fluid flow conditions of the reactions, i.e. laminar or turbulent [43][30]. Many combustion systems used for transportation and power generation operate in regimes where reactants are neither homogeneously mixed (i.e premixed flame) nor segregated on two sides of a contiguous (i.e diffusion flame). These modes have their own particular advantages and disadvantages [53]. Stratified combustion, in which a flame propagates through non-uniformly mixed reactants, is common in practical systems and in model combustors that have been designed to study relevant phenomena at atmospheric pressure [15]. Stratified combustion has found to result in reduced burned gas temperature, and thereby offers in a reduction of NO_X emissions [26, 39].

The premixed combustion has cleaner burnt products but it has a smaller range of operating conditions, making this mode of flame difficult to control [43]. On the divergent, having a wider operating range, a non-premixed combustion is easier to control [9, 26, 39]. Stratified combustion combines advantages of both premixed and non-premixed combustion modes [43, 44]. Lean stratified combustion can be further broken down into back- and front-supported regimes. Back-supported combustion occurs when the products are closer to stoichiometric than the reactants, and vice-versa for front-support.

It is acknowledged that there are many uncertainties about possible reaction initiation, propagation, and extinction mechanisms, and related phenomena. In addition, molecular diffusion, turbulence, radiation exchange, multi-phase, wall-surface, and catalytic effects are also important. A practical combustion system may have features and behavior that combine more than one of these idealized modes [6, 40].

1.2 Ignition

Ignition can be caused with the help of an external stimulus such as electric spark (SI engine), or due to high temperature without any external source (CI engine). Ignition not only initiates combustion but also influences subsequent combustion [2, 44]. Currently, the ignition process in most of the spark-ignition combustors is initiated by gaseous breakdown between a pair of high-voltage-applied electrodes. Such ignition schemes involve leaner fuel mixtures that require larger discharge energy, and higher initial pressure that requires higher voltage to be applied to the electrodes; both of which result in enhanced erosion of the electrodes and shorten the lifetime of the spark plug [50]. A successful ignition results in a high temperature region where the flame has outgrown the initial kernel. The ignition timing relative to the spark ignition will depend on the spark power, the thermo-physical properties of the fluids, density, and volatility of the droplets [30].

Localized ignition of both homogeneous and heterogeneous mixtures in the form of spark or laser plays an important role in the design of efficient Spark Ignition (SI) and Direct Ignition (DI) engines. Forced ignition in different combustion modes has been subject to numerous numerical analyses [11, 12, 38, 43]. Minimum Ignition Energy (MIE) is the energy that has to be deposited in the mixture in order to initiate a flame kernel which subsequently leads to self-sustained flame propagation. An increasing level of turbulence intensity, leads to high heat loss by diffusion due to intense disruption from eddies to the flame kernel, leading to an increase in MIE [44]. A parametric study of forced ignition at the mixing layer between air and air carrying fine mono-sized fuel droplets is done through direct numerical simulations [45, 46, 54]. The study helps to determine the influence of the spark location, the droplet-air mixing layer, initial thickness and the turbulence intensity on the ignition success and the subsequent flame propagation [3, 25, 41].

This thesis focuses on the source of localized forced ignition. The external source may be an electric spark or a laser. In the forced ignition, the initial condition is essentially chemically frozen and it is the deposition of energy and radical species that raises the temperature high and, quickly enough, creating a region wide enough for combustion to begin and providing a self-sustaining flame. The successfulness of ignition can be indicated by continued burning after the ignition source has been switched off [30, 44].

1.2.1 Different Ignition Sources

Spark Ignition

In spark-plug ignition, the duration of the electrical pulse applied to the electrodes is arbitrary in principle. However, if the pulse duration is too short, the electrical current becomes too large, and accordingly the lifetime of the electrodes becomes too short due to erosion [35]. The combustion process in a spark ignition engine is highly effected by the flame propagation and the turbulent flow in the combustion chamber.

Laser Ignition

In laser ignition, a gaseous medium is ignited by thermal and chemical effects of a small plasma, which is usually called a spark. A spark is created in a gaseous medium by laser-induced breakdown. Laser ignition displays attributes that may improve ignition, kernel development and flame propagation over conventional electric spark systems. Laser source ignition also produces overdriven flame speeds, demonstrated in quiescent homogeneous laser-ignited mixtures to produce flames that can momentarily propagate up to 20 times faster than the laminar flame speed [19].

Compression Ignition

When gases are compressed, heat is generated and thus, energy is transferred. If the rate of heat generation within a system exceeds the rate of heat loss (energy trans-

fer) to the surroundings, the temperature of the system will rise. The concept behind compression ignition involves using the latent heat built up by highly compressing air inside a combustion chamber as the means for igniting the fuel [1]. If the rate of compression is rapid enough such that the heat loss may be considered negligible, resulting in adiabatic compression, the temperature rise will depend on compression ratio [43].

Chemical Ignition

Pyrophoric fuels are one that ignite impulsively on contact with air or moisture, producing high rate of energy. Pyrophoric iron sulphides form when iron is exposed to hydrogen sulphide, or any other compound that contains sulphur, in an oxygen deficient atmosphere. They are found frequently in vessels, storage tanks, and sour gas pipelines. Pyrophoric iron sulphides present a hazard when equipment and tanks are opened for cleaning, inspection, and maintenance [43]. This type of ignition are uncommon in everyday life, but they are responsible for engine knock – the undesirable, erratic, and noisy combustion of low-octane fuels in internal combustion engines [47, 57].

1.3 Why Numerical Investigation?

Computational Fluid Dynamics (CFD) is the simulation of fluids engineering systems using modeling (mathematical physical problem formulation) and numerical methods [62]. CFD uses powerful computers and applied mathematics to model fluid flow situations. Several areas of CFD applications include architecture, chemical and process engineering, electronics and computer, HVAC (heat, ventilation & cooling), petroleum, train design, turbo machinery etc [52]. CFD enables analysts to simulate and understand fluid flows without the help of instruments for measuring various flow variables at desired locations [52]. The numerical solution is accepted at most of the times when the analytical solution of a defined problem is possible but it is

time consuming and the error of approximation is high. RANS (Reynolds averaged Navier–Stokes), LES (Large eddy simulation) and DNS (Direct numerical simulation) are one of the widely used numerical methods in combustion modeling. Numerical simulations are required to study the behavior of reacting flows whose mathematical models are too complex to provide analytical solutions, as in most nonlinear systems. Combustion process requires solving highly nonlinear Navier-Stokes equations with continuity and density transport equations for simulation, obtaining statistical flow solution [4, 58]. In recent times, Direct Numerical Simulation (DNS) has become an important tool for fundamental understanding and subsequent modeling of complex combustion phenomenon [29, 60].

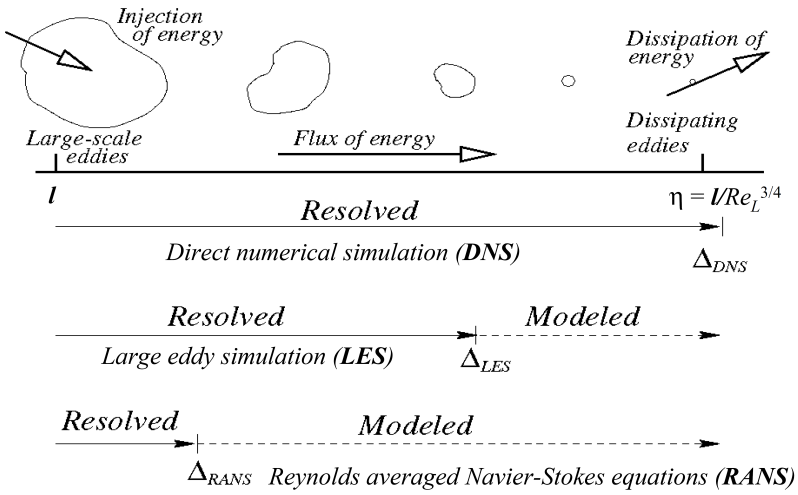

Figure 1.1: Simulation Methods [4]

Recent studies show increasingly reliant on computational fluid dynamics (CFD), which helps to evaluate the initial stages of the engine development. Direct Numerical Simulation (DNS) resolves all scales of motion, all the way down to the smallest turbulent scale. Large Eddy Simulation (LES) is next up and resolves most of the scales, with the smallest eddies being modeled [4](see figure 1.1). It aims to solve the computational cost that DNS poses and reveals the eddies hidden behind the mean in

RANS. Reynolds-averaged Navier-Stokes (RANS) is on the other end of the spectrum from DNS, where only the large-scale eddies are resolved and the remaining scales are modeled [4] (see figure 1.1). It is the least computationally expensive method that is used for turbulent modeling, but it is really not taken under consideration when certain phenomena cannot be averaged, such as instabilities [8].

Direct numerical simulations (DNS) for studying combustion process remains a very powerful tool in understanding interactions between chemistry, molecular transport and turbulence. The computational cost becomes more prohibitive, for more practical fuels. Direct numerical simulations (DNS) of combustion inside a cubical domain are performed in this thesis. DNS helps to extract the information which is difficult or impossible to obtain in the laboratory e.g. 3D temporal and spatial scales of time or vector scales, allowing a better understanding of the physics of turbulence. Also, DNS are useful in the development of turbulence models for practical applications, such as sub-grid scale models for large eddy simulation (LES) [4].

1.4 Research Motivation

In addition to premixed and non-premixed combustion, Peters mentions that partially premixed combustion plays, at least locally, an important role in technical applications [48]. Localized forced ignition of combustible inhomogeneous mixtures has a number of important applications ranging from Gasoline Direct Injection (GDI) engines to high-altitude relight in aero-gas turbines. An important example is modern gas turbine combustion chambers where fuel rich regions are used for flame stabilization but, in order to minimize NO_X formation, most of the combustion occurs under premixed fuel lean conditions. In numerous applications (internal combustion engines, industrial furnaces, gas turbine combustors, etc.), combustion through stratified mixtures is envisaged as a way of reducing fuel consumption by sustaining the combustion in a globally lean mixture [44]. A spatially non-homogeneous mixture

leads to changes in flame behavior in terms of heat release, propagation speed, this behavior is not well understood and has motivated the research reported in numerous studies. The characteristics of the combustion depend strongly on local variations of mixture and also on the length-scale of these variations. Devices like petrol fueled Otto-cycle engine used in most cars, reheat system fitted to jet engines for supersonic aircraft and modern industrial gas turbine engines for power generation rely mainly on premixed combustion [53].

The availability of detailed experimental data for model development and validation is very limited, and the state of modeling for stratified combustion is less advanced than that for non-premixed or fully premixed combustion. Furthermore, fundamental questions regarding the structure and dynamics of turbulent stratified flames remain unanswered. This influences to focus on DNS investigation of forced ignition process of turbulent combustible mixtures of both homogeneous and stratified fuel-air mixtures. In this study, effects of combustion regimes, fuel-air mixture inhomogeneity, and turbulence intensity were analyzed using three-dimensional DNS simulations. This new research direction includes investigating the different combustion regime where both chemistry and mixing are competitive during ignition which is more challenging. A deeper understanding of theoretical and numerical combustion with necessary equations will be an imperative splinter of this thesis.

1.5 Research Objectives

The study focuses on localized forced ignition of turbulent combustible mixtures. The main objectives of the thesis are:

• To understand the effects of combustion regimes on localized forced ignition of turbulent combustible mixtures.

• To understand the effects of Minimum Ignition Energy (MIE) on different turbulent combustion regime.

• To understand the effects of Karlovitz number (Ka) with mixture inhomogeneity on turbulent combustion where flame is originated from localized forced ignition.

• To compare favorable conditions between homogeneous and stratified turbulent mixture for burned gas mass.

Chapter 2

Literature Background

This chapter introduces the combustion modes from various means, i.e both experimentally and numerically. The chapter provides a review of premixed flame structure and forced ignition of homogeneous and inhomogeneous mixtures. Additionally the chapter reflects on the recent studies available in the literature.

2.1 Forced Ignition of Homogeneous and Inhomogeneous mixtures

It is very important to distinguish the different phases involved in the ignition process. The different phases of ignition process can be summarized as [35, 37, 38]

1. Flame kernel generation
2. Flame growth
3. Successful ignition

The boundaries between these phases are not always clear and this is manifested by the different interpretations given to the term ignition in the literature. The flame kernel would normally be small, of the order of the spark size. The flame growth would normally occur over length scales of the order of the integral length scale and over timescales comparable to some bulk flow timescale [38]. Following to this phase,

the flame kernel growth slows down and the thermal spread is now supported by the spark energy. When sufficient heat has been lost to the fresh mixture thereby the flame kernel temperature has dropped near to adiabatic flame temperature T_{ad}, its size will determine in self propagating flame kernel. By this stage, the heat release has to overcome the heat transfer by the flame kernel if the flame kernel reaches to a critical size [35]. The third phase, full burner ignition, where kernel growth is determined by the heat release and becomes self propagating flame, thereby attaining the successful ignition process [38, 43].

2.2 Premixed flame structure

A premixed flame can occur when the fuel and oxidizer are mixed together before ignition. In principle, the mixing between fuel and oxidizer should be complete to the molecular level before combustion takes place, although some degree of mixture inhomogeneity is normal in practical system [5, 35]. The most important behavioral characteristic of premixed flames is propagation. A premixed flame moves spontaneously in a direction normal to itself in order to consume the available reactant mixture [9, 53]. This is in contrast to non-premixed flame which must remain attached to the stoichiometric surface between the fuel and the oxidizer, although the surface itself may be convicted from place to place by the local flow field [43]. This thesis focuses on the flame propagation in stratified mixture taking fill advantage of flammability limit.

The generic structure of a laminar premixed flame is shown in figure 2.1. The area of flame front is divided into three distinct zones; preheat zone, reaction zone and equilibration zone defined by Zel'dovich and Frank-Kamenetzki [9].

2.2.1 Preheat Zone

The temperature of the reactants (T_R) increases due to the diffusion of heat from the reaction zone. No chemical reaction occurs in this zone and heat release has been

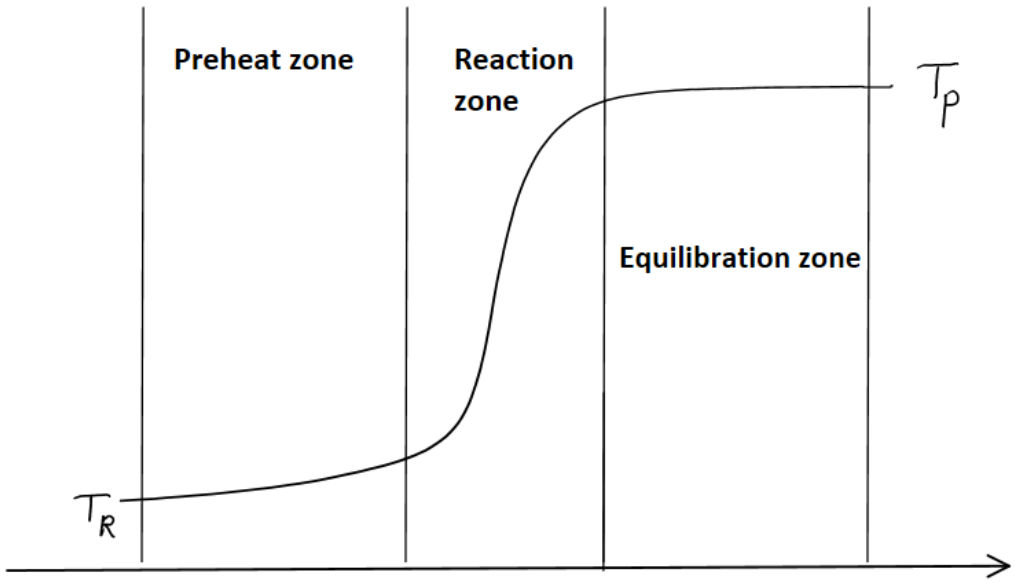

Figure 2.1: General structure of laminar premixed flame

neglected.

2.2.2 Reaction Zone

The chemical energy is released in the form of heat here due to chemical reaction. With the heat release, the temperature gradient is high in this zone. It is very thin and constitutes of overlapping reaction and diffusion layers.

2.2.3 Equilibration Zone

Formation of $C0_2$ and H_2O, along with the heat release occurs in this zone. It is comparatively thicker than reaction zone and not much chemical reaction takes place as chemical equilibrium is achieved in this zone. The temperature of the products T_P is extremely high in comparison to T_R.

Existing literature suggests that, the reaction zone thickness for most hydrocarbon fuels is less than a millimeter, and the entire flame thickness is rarely more than a few millimeters. [9].

2.3 Turbulent Length and Time Scale

The largest length scale of turbulence is known as the integral length scale (i.e L_{11}), which is the length scale at which most of the large eddies are associated (see figure 1.1). By contrast, the smallest length scale of turbulence known as Kolmogorov length scale (i.e η), is determined by viscous dissipation of turbulent kinetic energy. From Kolmogorov's hypothesis, [9, 44] the only factors influencing the behavior of the small scale motions are the overall kinetic energy dissipation rate (ε) and the viscosity (ν). The length scale which governs these physical mechanisms is given by:

$$\eta = \left(\frac{\nu^3}{\varepsilon}\right)^{\frac{1}{4}} \tag{2.1}$$

To relate this length scale to the largest length scale in the flow, it requires an estimation for the dissipation rate in terms of the large scale flow features. The kinetic energy of the flow is proportional to $(u')^2$, RMS turbulence intensity. The time scale of the life time of the large eddies (commonly referred to as the large eddy turnover time) can be estimated as $\frac{L_{11}}{u'}$. Thus, it is assumed that the kinetic energy dissipation rate scales as [43]:

$$\varepsilon = \frac{(u')^3}{L_{11}} \tag{2.2}$$

Therefore, it can be written as,

$$\eta = \left(\frac{\nu^3 L_{11}}{u'^3}\right)^{1/4} \tag{2.3}$$

The ratio of the largest to smallest length scales in the turbulent flow is given by:

$$\frac{L_{11}}{\eta} \sim \left(\frac{u' L_{11}}{\nu}\right)^{3/4} \sim Re_t^{3/4} \tag{2.4}$$

where $Re_t \sim \left(\frac{u' L_{11}}{\nu}\right)$ is the turbulent Reynolds number.

The large eddy turnover time (t_e) is defined by:

$$t_e \sim \frac{L_{11}}{u'} \tag{2.5}$$

All the simulations in this thesis accounts for at least two eddy turn over time in order to capture turbulence resolution.

The life time for the small eddies of turbulence can be estimated using the viscosity and the dissipation rate [43]:

$$t_\eta = \left(\frac{\nu}{\epsilon}\right)^{1/2} \tag{2.6}$$

Thereby, using Eq. 2.2

$$t_\eta = \left(\frac{\nu L_{11}}{u'^3}\right) \tag{2.7}$$

The ratio of time scales are given by,

$$\frac{t_e}{t_\eta} = \left(\frac{u' L_{11}}{\nu}\right)^{1/2} = Re_t^{1/2} \tag{2.8}$$

As the turbulent Reynolds number of the flow increases, the magnitude of the separation between both time and length scale increases.

2.4 Karlovitz Number

The Karlovitz number (Ka) is a dimensionless parameter and is used in turbulent combustion and corresponds to the ratio of chemical time scale t_f and smallest turbulent time scale t_η (i.e Kolmogorov time scale)

$$Ka = \frac{t_f}{t_\eta} \tag{2.9}$$

where t_η is life time for smallest eddy (see eqn 2.7)

$$Ka = f\left(\frac{u'}{S_b}, \frac{L_{11}}{l_f}\right) \tag{2.10}$$

Flame-turbulence interaction in turbulent premixed combustion can be characterized using [51]:

$$Ka = \frac{[u'/S_{b(\phi)}]^{3/2}}{\sqrt{L_{11}/l_f}} \tag{2.11}$$

Turbulence do not alter the flame structure and the chemical region is in laminar conditions [49, 51].

2.5 Regime Diagram

Various types of flame-turbulence interaction can be summarized on a regime diagram for the turbulent combustion [9]. Regime for premixed turbulent combustion is defined in terms of velocity and length scale ratio [9, 43]. Four turbulent combustion regimes have been identified. They include: (1) Wrinkled Flamelet regime, (2) Corrugated regime, (3) Thin Reaction Zone regime and (4) Broken Reaction regime. Transitions from different regimes are achieved through variations of the vortex strength, and operation in each regime is governed by two key parameters, the ratio of the vortex translational velocity to the laminar flame speed and the ratio of the kernel size to the vortex size at the onset of the interactions. A combustion regime often refers to the outcome of competitions between length, time and velocity scales, which characterize turbulence, chemistry and their coupling [9]. This competition may result in thin flame structures, or flamelets, that are wrinkled and adverted by the turbulent flow, with little effects of the turbulence on their structures [16].

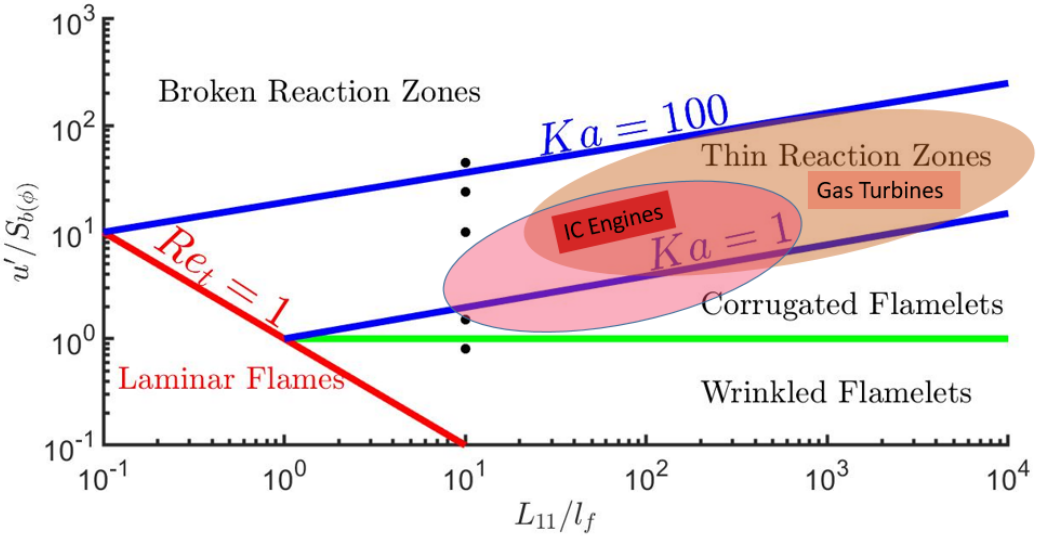

Figure 2.2: Regime diagram for premixed turbulent combustion representing the areas for engineering applications and indicating simulation cases for present study [9]

For scaling purposes it is useful to assume a Schmidt number $Sc = \nu/D$ to unity and to define the flame thickness (l_f), Zel'dovich flame thickness as,

$$l_f = \frac{D}{S_b(\phi)} \tag{2.12}$$

Using the turbulent velocity, u' and the integral length scale L_{11}, one can estimate the turbulent Reynolds number as:

$$Re_t \sim \frac{u'}{S_{b(\phi)} l_f} \tag{2.13}$$

Furthermore, one can quantify the separation between chemical time scale to the Kolmogorov scale in the following manner:

$$Ka \sim \frac{t_f}{t_\eta} \sim \frac{l_f^2}{\eta^2} \tag{2.14}$$

Now, using the definition of Komogorov length scale, where the ratios $u'/S_{b(\phi)}$ and

L_{11}/l_f may be expressed in terms of the two dimensional numbers Re_t and Ka as:

$$\frac{u'}{S_{b(\phi)}} = Re\left(\frac{L_{11}}{l_f}\right)^{-1} = Ka^{2/3}\left(\frac{L_{11}}{l_f}\right)^{1/3} \tag{2.15}$$

The diagram (see figure 2.2) is divided into specific regions by lines representing values of the turbulent Reynolds number (Re_t) and Karlovitz number (Ka). In this diagram, the lines $Re_t = 1$, $Ka = 1$ and $Ka = 100$ represent boundaries between the different regimes of premixed turbulent combustion. Another boundary of interest is the line $u'/S_{b(\phi)}$, which separates the wrinkled and corrugated flamelets and the line denoted by $Ka = 100$, which separates thin reaction zones from broken reaction zones. The line $Re_t = 1$ separates all turbulent flame regimes from the regime of laminar flames, which is situated in the lower-left corner of the diagram. The laminar flamelet regime occupies the region of diagram where the turbulent Reynolds number is high and Karlovitz number is low, indicating moderately strong turbulence with fast chemistry and low turbulent strain rates. The flamelet regime is subdivided into the regimes of wrinkled and corrugated flamelets, which is characterized by the inequalities $Re_t > 1$ (turbulence) [9]. In the wrinkled flamelet regime, where $u' < S_{b(\phi)}$, u' may be interpreted as the turnover velocity of the large eddies. In the regime of corrugated flamelets there is an interaction between turbulent and laminar flame propagation. Since the velocity of large eddies is larger than the burning velocity, these eddies will push the flame around, causing a substantial corrugation. Conversely, the smallest eddies, having a turnover velocity less than the burning velocity, will not wrinkle the flame [9, 31, 48, 56]. The boundary to the thin reaction zones regime is given by $Ka = 1$, which, according to (2.11), is equivalent to the condition that the flame thickness is equal to the Kolmogorov scale. The thin reaction zones regime is characterized by $Re_t > 1$, $Ka < 100$ and $Ka > 1$, the last inequality indicating that the smallest eddies can enter into the flame structure since $\eta < l_f$. Beyond the line $Ka = 100$, is the broken reaction zone. In this regime, the Kolmogorov eddies

enter into the inner layer and thereby the chemical processes are disturbed locally. This leads to heat loss to the preheat zone followed by temperature decrease, which eventually results in flame extinguish.

2.6 The Researchers' View

Many numerical studies have focused on either premixed or non-premixed combustion from various researchers [24, 28, 42, 44, 55]. A number of numerical studies have examined the behavior of partially premixed and stratified flames, from 1D laminar to 3D turbulent flows. Computational models that are simple extensions of premixed modeling approaches have been applied to stratified systems with some success and more extensive approaches bridging regimes have also been proposed. Harworth [24] have shown that in partially premixed systems, combustion occurs in two stages: a primary flame that consumes all primary reactants and produces most of the heat release, and a secondary reaction zone, behind the primary flame, where combustion products, fuel excess from rich zones, and oxidizer excess from lean zones mix. Literature [24, 28] on stratified combustion has generated contradictory results because the effects of mixture stratification on combustion depend greatly on the mixture distribution and on the definition of an equivalent homogeneous mixture for a relevant comparison. Jimenez [28] have shown that the different effects induced by mixture inhomogeneities (variation in local reaction rate and in heat release, interaction with turbulent flow, temperature, and composition of burned gases) can lead individually to an increase or decrease in heat release. The distribution of mixture inhomogeneities in space and their variation in magnitude will control the competition between these different effects and can lead to different behavior concerning propagation and efficiency [28]. The effect of stratification on low turbulence, Re_t lean flames has been investigated recently in a small number of studies [18, 23, 43]. Renou [42, 55] studied the behavior of unsteady flame kernels propagating through

carefully tailored equivalence ratio gradients in overall lean flames. They found that stratification increased the mean curvature of the flames, as well as their wrinkling relative to premixed flames. Pasquier [42] studied the propagation of flames through stratified lean turbulent propane mixtures in a combustion bomb. The results showed that flame propagation was influenced by the stoichiometry of the mixture, showing that locally lean mixtures burn faster.

From the literature study [28, 42, 43, 55], it is been observed that stratified mixtures shows more promising option as compared to homogeneous mixtures for sustainable combustion. A deeper understanding of this effects with different parameters on stratified mixtures will be the focus of this thesis.

Chapter 3

Mathematical Background and Numerical Implementation

This chapter presents the mathematical formulations and numerical implementations along with the assumptions taken in this thesis.

3.1 Governing Equation

All the simulations presented in this thesis are performed using a well known compressible DNS code SENGA [13]. This DNS code solves the full compressible Navier Stokes equations on a cartesian grid [44]. The governing equation that describes the three dimensional gaseous reacting flow consists of mass, momentum, energy and species conservation equations. These equations in dimensional form are [9, 43]:
Mass Conservation Equation:

$$\frac{\partial}{\partial t}\rho + \frac{\partial}{\partial x_j}\rho u_j = 0 \tag{3.1}$$

Momentum Conservation Equation:

$$\frac{\partial}{\partial t}\rho u_i + \frac{\partial}{\partial x_j}\rho u_j u_i = -\frac{\partial}{\partial x_i}P + \frac{\partial}{\partial x_j}\tau_{ji} \tag{3.2}$$

where viscous stress tensor τ_{ij} is defined as:

$$\tau_{ij} = \mu\left[\left(\frac{\partial u_i}{\partial x_j} + \frac{\partial u_j}{\partial x_i}\right) - \frac{2}{3}\delta_{ij}\frac{\partial u_k}{\partial x_k}\right] \tag{3.3}$$

Energy Conservation Equation:

$$\frac{\partial}{\partial t}\rho E + \frac{\partial}{\partial x_k}\rho u_k E = -\frac{\partial}{\partial x_k}u_k P + \frac{\partial}{\partial x_k}\tau_{ki}u_i + \frac{\partial}{\partial x_k}\left[\lambda_o\frac{\partial \hat{T}}{\partial x_k}\right] + \dot{w}_T \tag{3.4}$$

Species Conservation Equation:

$$\frac{\partial}{\partial t}\rho Y_\alpha + \frac{\partial}{\partial x_j}\rho Y_\alpha u_j = \dot{w}_\alpha - \frac{\partial}{\partial x_j}\rho Y_\alpha V_{\alpha j} \qquad \text{where } \alpha = 1, 2...N \tag{3.5}$$

In the above equations, ρ is the density, u_i is the i^{th} component of the velocity vector, P is the pressure, E is the stagnation internal energy, λ_o is the thermal conductivity, $\hat{T}$ is the temperature, h_α is the enthalpy of formation of the species α and $V_{\alpha j}$ is the diffusion velocity of the species α depending on the mixture and Y_α is the mass fraction of the species α in the reacting mixture containing total number of species N. The source term $\dot{w}_T$ originating from the heat release due to combustion is defined as:

$$\dot{w}_T = H_\phi|\dot{w}_F| \tag{3.6}$$

where H_ϕ is the heat released per unit mass of fuel and $|\dot{w}_F|$ represents normalized fuel reaction rate magnitude.

3.2 Assumptions in Numerical Investigation

The following assumptions are taken under consideration for the given analysis :

1. The chemical mechanism is simplified here by single step chemical reaction,

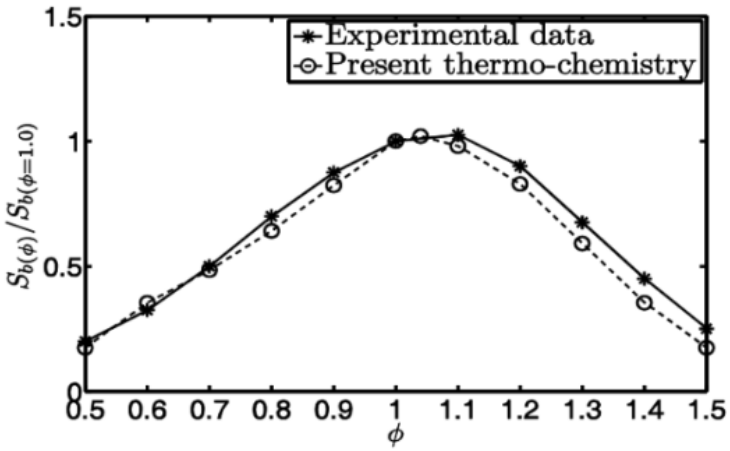

Figure 3.1: The variation of laminar burning velocity $\frac{S_{b(\phi)}}{S_{b(\phi=1.0)}}$ with equivalence ratio ϕ for the present thermo-chemistry along with the experimental variation [17, 43]

which takes the following form [21, 44]:

$$Fuel + s \cdot Oxidiser \rightarrow (1+s) \cdot Products \tag{3.7}$$

where s indicates the mass of the oxidiser consumed per unit mass of fuel consumption under stoichiometric conditions.

2. The reactants are fuel and oxidiser, where the fuel reaction rate is expressed as:

$$\dot{w}_F = -\rho B^* Y_F Y_O exp\Big[-\frac{\beta(1-T)}{1-\alpha(1-T)}\Big] \tag{3.8}$$

where ρ is the gas density and the non dimensional temperature $T = \frac{\hat{T}-T_0}{T_{ad}-T_0}$ where $\hat{T}$ is the instantaneous dimensional temperature, T_O is the initial reactant temperature and T_{ad} is the adiabatic flame temperature for stoichiometric mixture.

Zel'dovich number:

$$\beta = \frac{E_{ac}(T_{ad}-T_0)}{R_0 T_{ad}^2} \tag{3.9}$$

Heat release parameter :

$$\alpha = \frac{\tau}{1+\tau} = \frac{(T_{ad} - T_0)}{T_{ad}} \tag{3.10}$$

pre-exponential factor related constant:

$$B^* = B \exp\left(- \frac{\beta}{\alpha} \right) \tag{3.11}$$

where E_{ac} is the activation energy, B is the pre-exponential factor and τ is the heat release parameter.

3. The activation energy (E_{ac}) and heat of combustion are taken to be function of ϕ [21], so the realistic ϕ dependence of unstrained laminar burning velocity $S_{b(\phi)}$ can be obtained. The equivalence ratio ϕ can be expressed as $\phi = \frac{FAR}{(FAR)_{st}}$, where FAR and $(FAR)_{st}$ are the actual and stoichiometric air-fuel ratio. The normalized laminar burning velocity $S_{b(\phi)}/S_{b(\phi=1)}$ variation with equivalence ratio ϕ is shown in Fig. 3.1, which shows that the present thermo-chemistry satisfactorily apprehends the experimentally obtained laminar burning velocity variation with equivalence ration (ϕ) for typical hydrocarbon-air mixtures [17]. The heat release per unit mass of fuel $H_\phi = \frac{[T_{ad(\phi)} - T_O] C_P}{(Y_{Fu(\phi)} - Y_{Fb(\phi)})}$ is given by:

$$\frac{H_\phi}{H_{\phi=1}} = \begin{cases} 1 & \phi \leq 1 \\ 1 - \alpha_H(\phi - 1) & \phi > 1 \end{cases} \tag{3.12}$$

where $\alpha_H = 0.21$ for CH_4-Air flames [21], $Y_{Fu(\phi)}$ and $Y_{Fb(\phi)}$ is the fuel mass fraction in the unburned and the burned gas respectively for premixed flame corresponding to the ϕ and C_P is the specific heat at constant pressure.

4. The transport quantities such as viscosity, thermal conductivity and the density-

weighted mass diffusivity are taken to the same for all species and independent of temperature. The combustion is assumed to be taking place where all species are perfect gases, which follows following relations:

Stagnation internal energy:

$$E = C_V \hat{T} + \frac{1}{2} u_k u_k \tag{3.13}$$

Pressure:

$$P = \rho R_O \hat{T} \tag{3.14}$$

Gas constant:

$$R_O = C_P - C_V = (\gamma - 1) C_V \tag{3.15}$$

Ratio of specific heats:

$$\gamma = \frac{C_P}{C_V} = 1.4 \tag{3.16}$$

Prandtl number:

$$Pr = \frac{\mu C_P}{\lambda_O} = 0.7 \tag{3.17}$$

Schmidt number:

$$Sc = \frac{\mu}{\rho D} \tag{3.18}$$

and Reynolds number:

$$Re = \frac{\rho u l}{\mu} \tag{3.19}$$

3.3 Ignition Modeling

The heat addition by the igniter is accounted for by adding an additional source term q''' in the energy transport equation in the following manner [9]:

$$\frac{\partial}{\partial t}\rho E + \frac{\partial}{\partial x_k}\rho u_k E = -\frac{\partial}{\partial x_k}u_k P + \frac{\partial}{\partial x_k}\tau_{ki}u_i + \frac{\partial}{\partial x_k}\left[\lambda\frac{\partial \hat{T}}{\partial x_k}\right] + \dot{w}_T + \underbrace{q'''}_{\text{source term}} \tag{3.20}$$

where $\dot{w}_T$ is the source term originating from heat release due to combustion. The expression for the specific stagnation internal energy E is given by:

$$E = \int_{T_O}^{\hat{T}} C_V dT + \frac{u_k \cdot u_k}{2} \tag{3.21}$$

The source term q''' is assumed to follow a Gaussian distribution in the radial direction away from the center of the igniter [44] and is expressed as:

$$q'''(r) = A_q \cdot exp\left(-\frac{r^2}{2R^2}\right) \tag{3.22}$$

where r is the radial direction from the center of the igniter and R is the width of the Gaussian profile[12]. This choice of R allows for sufficient resolutions of the temperature gradient and guarantees the rapid disappearance of any artificial effects introduced by the ignition source. In equation (4.28), the constant A_q is determined by the following volume integration :

$$\dot{Q} = \int_v q''' dV \tag{3.23}$$

where $\dot{Q}$ is the ignition power, which is defined as :

$$\dot{Q} = a_{sp}\,\rho_0\,C_P\,\tau\,T_0\,(4\pi l_f^3/3)\left(\frac{H(t) - H(t - t_{sp})}{t_{sp}}\right) \tag{3.24}$$

where τ is the heat release parameter [44]. The parameter a_{sp} determines the total energy deposited by the igniter and the Heaviside function $H(t)$ and $H(t - t_{sp})$

ensure the ignition source term remains operational for the energy deposition time during duration t_{sp}. The parameter t_{sp} can be expressed as $t_{sp} = b_{sp}t_f$, where b_{sp} is the energy deposition duration parameter and $t_f = l_f/S_{b(\phi=1)}$ is the characteristic chemical time scale. All the simulations are carried out to $10.5t_{sp}$.

The igniter is placed at the center of the computational domain and the ignition model used here only addresses the thermal aspect of the localized forced ignition and the details of spark formation (momentum modification contribution and shock wave) are kept beyond the scope of the present analysis to keep it computationally feasible.

3.4 Mixture fraction

Fuel mass fraction Y_F and mixture fraction ξ are involved for describing the turbulent combustion of stratified mixtures [36]. The mixture fraction is expressed using fuel and oxidizer mass fraction as [7]:

$$\xi = \frac{Y_F - \frac{Y_O}{s} + \frac{Y_{O\infty}}{s}}{Y_{F\infty} + \frac{Y_{O\infty}}{s}} \tag{3.25}$$

where Y_F and Y_O are local fuel and oxidizer mass fractions, $Y_{F\infty}$ is the fuel mass fraction in the pure fuel stream and $Y_{O\infty}$ is the oxidizer mass fraction in air. The equivalence ratio ϕ can be expressed in terms of ξ using Burke-Schumann solution [49] as:

$$\phi = \frac{1-\xi_{st}}{\xi_{st}} \times \frac{\xi}{1-\xi} \tag{3.26}$$

where $\xi_{st} = \frac{Y_{O\infty}}{sY_{F\infty}+Y_{O\infty}}$ is the extent of of the completion of the chemical reaction can be characterized by a reaction progress variable c which is defined as:[7]

$$c = \frac{\xi Y_{F\alpha} - Y_F}{\xi Y_{F\alpha} - \max[0, \frac{\xi-\xi_{st}}{1-\xi_{st}}]Y_{F\alpha}} \tag{3.27}$$

In the present analysis, $\xi_{st} = 0.055$ (AFR_{st}=17.16) represents methane-air binary

mixture. The extent of the completion of the chemical reaction is quantified using a reaction progress variable c, where Y_{Fu} and Y_{Fb} are the fuel mass fractions in the unburned and burned gases respectively. According to the equation, c rises monotonically from zero in the fully unburned reactants to one in the fully burned products.

3.5 Mixture inhomogeneity length scale

The taylor micro- scale of the equivalence ratio variation is defined as [20, 43]:

$$l_\phi = \sqrt{\frac{6 < [\phi - < \phi >]^2 >}{< \nabla[\phi - < \phi >] \cdot \nabla[\phi - < \phi >] >}} \tag{3.28}$$

where l_ϕ represent length scale of mixture inhomogeneity and the angle brackets indicate the global mean evaluated over the whole of the computational domain.

3.6 Resolution of Scales

For the principle of turbulent combustion simulations, DNS grids must follow the following essentials:[44]

1. Total number of grid points in DNS should be large enough to ensure the largest scales of flow are captured and enough number of samples, which then can be used for obtaining statistically converged results.

2. DNS mesh should be fine enough to ensure that the smallest scales of flow (i.e. the Kolmogorov length scale) are fully resolved.

3.6.1 Turbulent Scale

A turbulent flow can be considered to be fully resolved when the smallest scale of flow are fully resolved by the computational mesh. A cubical computational domain with side length L requires $N_g + 1$ grid points on each sides for full resolved flow in DNS with cell size of $\triangle x = \frac{L}{N_g}$. The cell size needs to be smaller than Kolmogorov scale,

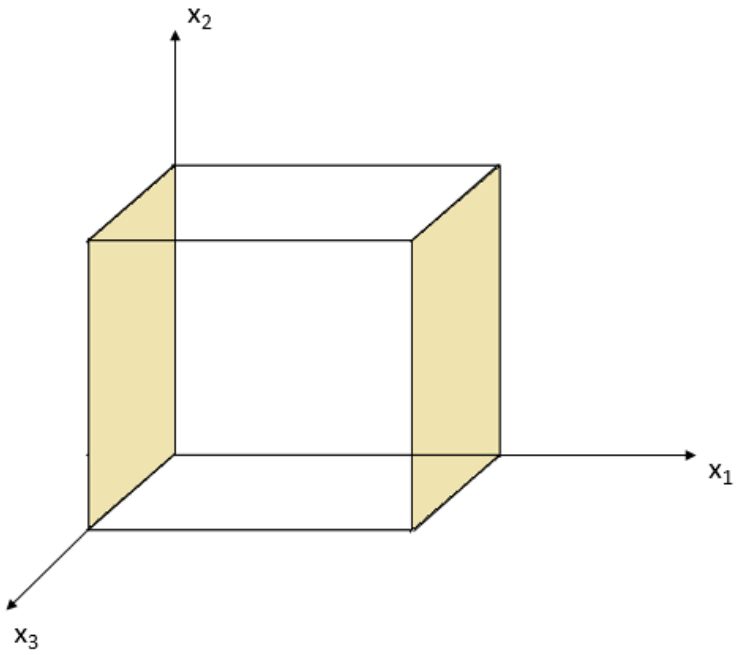

Figure 3.2: Inflow and outflow boundaries

thereby [43]:

$$\frac{L_{11}}{\eta} < N_g \tag{3.29}$$

where, η is the Kolmogorov length scale and L_{11} is the integral length scale. In the present study, the uniform grid spacing $\triangle x$ is smaller than Kolmogorov length scale η ($\eta \geq 1.2\triangle x$).

3.6.2 Chemical Scale

Resolution of the chemical structure is also an essential segment of the DNS. Thereby, the computational mesh should resolve the inner flame structure. The study adopts simplified Arrhenius-type chemistry and the inner flame should extent over about 10 grid points. The flame thickness δ_{th} must expand over Q elementary cells and in terms of the flame thickness, computational length L can be shown as, $L \approx \frac{N_g}{Q}\delta_{th}$.

For all simulations performed in this present thesis, a compressible three-dimensional DNS code SENGA [28] was used to carry out the simulations, been run for a duration

of $10.5t_{sp}$ under decaying turbulence in a domain of size $51l_f \times 51l_f \times 51l_f$, which further discretized by a Cartesian grid of size $310 \times 310 \times 310$ with uniform grid spacing ensuring at least 10 grid points within the thermal flame thickness of the stoichiometric laminar flame as:

$$\delta_{th(\phi=1)} = \frac{\left[T_{as(\phi=1)} - T_0\right]}{\left[\max\left|\nabla \hat{T}\right|_L\right]} \tag{3.30}$$

where $\hat{T}$ is the instantaneous temperature.

3.7 Boundary Conditions

A combustible mixture in a cubic domain is ignited in the center of the cube and a flame kernel is allowed to expand and freely propagate. The boundaries in the x_1-direction are taken to be partially non-reflecting and specified by the Navier Stokes Characteristic Boundary Conditions (NSCBC) as shown in figure 3.2, described by Poinsot and Lele [35, 51]. The other boundaries are considered to be periodic in nature. The boundaries in the transverse direction are considered to be periodic in nature.

Chapter 4

Results and Discussion

The following chapter displays the DNS results of the present study where the flame is originating from the igniter and freely propagating in both turbulent homogeneous and stratified mixture environment.

Simulation Parameters

Table 4.1: Simulation parameters

			Stratified mixture $\phi' = 0.2, <\phi>= 1.0$			Homogeneous
	Ka	$\frac{L_{11}}{l_f} = 10$	$\frac{l_\phi}{l_f} = 1.6$ [A]	$\frac{l_\phi}{l_f} = 2.5$ [B]	$\frac{l_\phi}{l_f} = 4.5$ [C]	
$\phi = 1.0$	0.052	$\frac{u'}{S_{b(\phi)}} = 0.8$	WFA	WFB	WFC	HWF
	0.226	$\frac{u'}{S_{b(\phi)}} = 1.5$	CFA	CFB	CFC	HCF
	10	$\frac{u'}{S_{b(\phi)}} = 10$	10TRA	10TRB	10TRC	H10TR
	37.2	$\frac{u'}{S_{b(\phi)}} = 24$	24TRA	24TRB	24TRC	H24TR
$\phi = 0.5$	120	$\frac{u'}{S_{b(\phi)}} = 41.6$	BRA	BRB	BRC	HBR

All the simulations parameters of this thesis is listed in the Table 4.1. Table 4.1 shows the parametric variation of $\frac{l_\phi}{l_f}$, $\frac{u'}{S_{b(\phi)}}$, ϕ and Ka and thereby in total of 20 simulations (15 stratified cases + 5 homogeneous cases) have been conducted here. The case names are given by considering the different regime[48] as mentioned in section [2.4] figure 2.2, such that WF stands for Wrinkled flamelet, CF stands for Corrugated flamelet, TR stands for Thin reaction zone and BR is Broken reaction zone; A, B and C denote the increasing values of l_ϕ/l_f; H represents the Homogeneous mixtures (e.g 10TRA corresponds to case for globally stoichiometric stratified mixture with initial values of $u'/S_{b(\phi=1)} = 10$; $l_\phi/l_f = 1.6$; Thin reaction zone regime). For the present thesis, the ignition parameter are selected as $b_{sp} = 0.2$ and $R \simeq 1.55 l_f$ and $a_{sp} = 7.35$ for the cases WF, CF and 10TR; $a_{sp} = 12.86$ for the case 24TR; $a_{sp} = 11.02$ for the case BR. Since laminar burning velocity is observed to be maximum in region $1.0 < \phi < 1.1$ (see figure 3.1) where $\phi' = 0.2$ has been chosen to highlight maximum burning velocity area [44, 45]. All the simulations have been carried out for $t = 10.5 t_{sp} = 2.1 t_f$, ($t_f$ = characteristic chemical scale).

4.1 Effects of Minimum Ignition Energy (MIE) in different combustion regime

In this section the effects of energy deposition a_{sp} on localized forced ignition of homogeneous mixtures have been analyzed, their results are shown and subsequently discussed. The results supports on selection of favorable value of a_{sp}, which lead to successful ignition and further self-sustained combustion.

The temporal evolution of the maximum non-dimensional temperature (T_{max}) and the corresponding turbulence decay profile for all the homogeneous cases listed in the Table 4.1 are shown in the figure 4.1., where [43]:

$$T_{max} = \frac{\hat{T}_{max} - T_0}{T_{ad(\phi=1)} - T_0} \qquad \text{for } \phi = 1.0 \text{ mixtures} \tag{4.1}$$

$$T_{max} = \frac{\hat{T}_{max} - T_0}{T_{ad(\phi=0.5)} - T_0} \qquad \text{for } \phi = 0.5 \text{ mixtures} \tag{4.2}$$

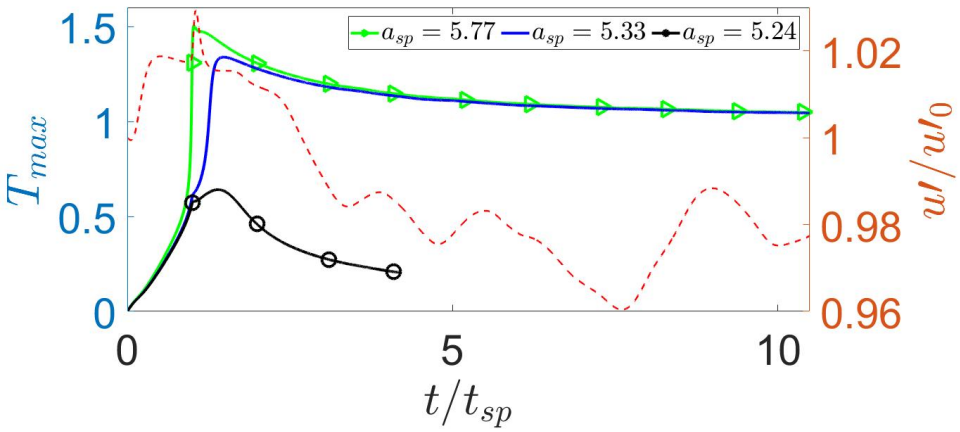

Case 1: WF

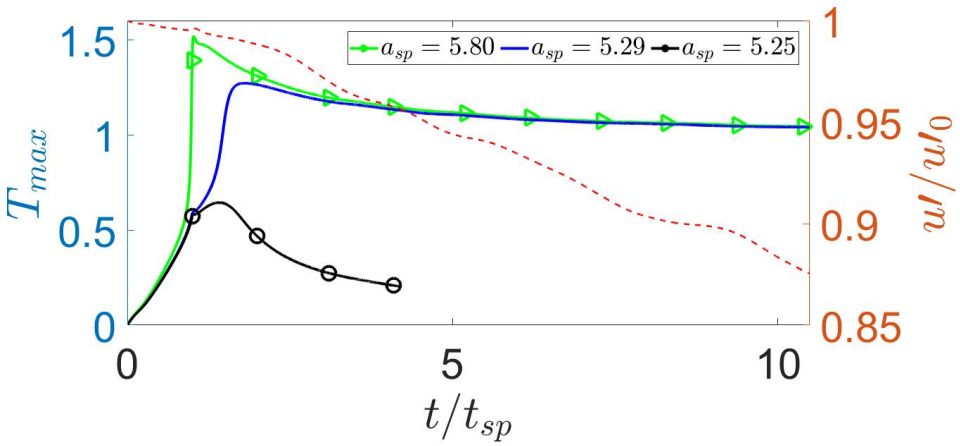

Case 2: CF

Figure 4.1 shows the T_{max} profile for the homogeneous mixtures on the effects of ignition energy, a_{sp}. It can be seen that the T_{max} rises with time during energy deposition $0 \leq t \leq t_{sp}$ and thermal escape takes place when T_{max} reaches value very close to critical temperature, i.e $T_c \approx 1 - (1/\beta)$, and thereby T_{max} rises rapidly at this mark. The value of T_{max} gradually decreases after $t = t_{sp}$, i.e after the igniter

is switched off, and attains adiabatic temperature ($T_{ad} \approx 1.0$) suggesting successful ignition followed up by self-sustained combustion has been achieved.

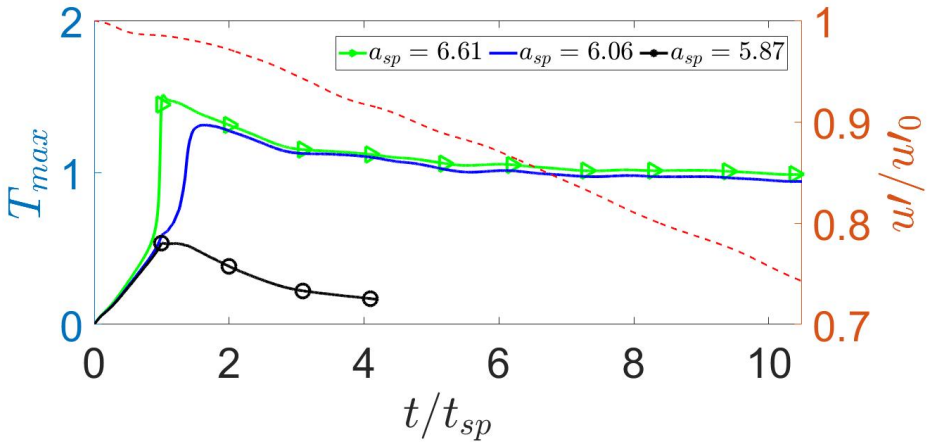

Case 3: TR

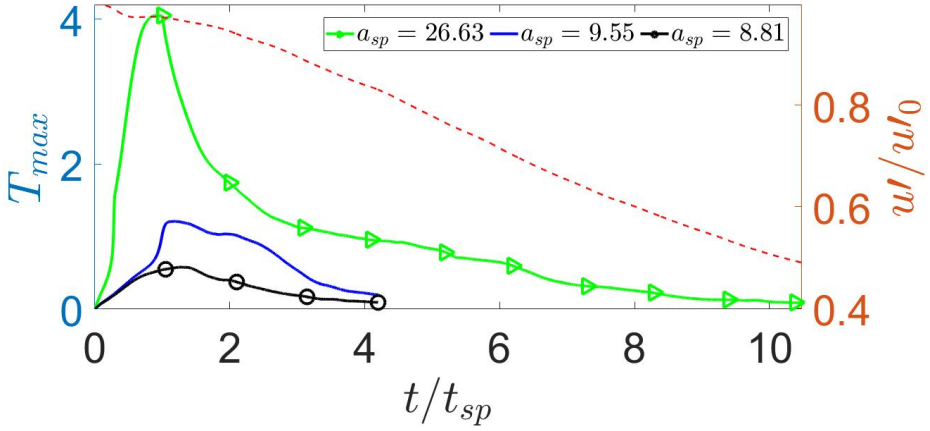

Case 4: BR

Figure 4.1: Temporal evolution of T_{max} and the corresponding turbulence decay profile for the cases WF, CF, TR, BR respectively

The profiles in – ▶ – (except the case BR for $a_{sp} = 26.63$) represents successful ignition followed up by self-sustained combustion, by procuring adiabatic temperature (T_{ad}). The profiles in – for all the cases approach to the temperature where self sustained combustion is been seen but with delay in ignition, are observed only till $t = 4t_{sp}$ and this time interval is sufficient to analyze the ignition behavior. The temperature increases with lesser acclivity, and the ignition is achieved around $1.5t_{sp}$ for all the cases, showing that the value of energy deposition ignites the mixture but not sufficient enough to ignite the particular mixture composition by the time interval of $t = t_{sp}$. The profile in – ∘ – shows the choice of a_{sp} is not enough to even ignite the mixture, thereby can be treated as critical value of ignition energy for given condition of Ka and this results shows good agreement with previous literature [45, 46].

Successful ignition with self sustained combustion was seen in all the cases (except the case BR). The smallest value of a_{sp} for the given cases indicates the minimum amount of energy required to ignite the mixture, but does not guarantee self-sustained combustion. The amount of ignition energy resulting in self sustained combustion is different from the the amount of ignition energy which simply just ignites the mixtures, therefore careful selection of igniter is necessary for different applications.

It can be seen in the figure 4.1 that the cases CF required the least MIE to achieve successful ignition and self sustained combustion, and also the turbulence decay is much smoother as compared to the case WF. Increase in turbulence intensity at initial stages for the case WF is seen in the figure 4.1. The $\frac{u'}{S_{b(\phi=1)}}$ value where it shows that turbulent eddies are not strong enough to penetrate into flame structure, however, the igniter gives rise to shock and plasma waves which further increases the turbulence intensity within the domain (observed in $\frac{u'}{u'_0}$) which shows abrupt behavior. In case BR, successful ignitions occurs, however it is difficult to attain self-sustained combustion due to high turbulence. This reveals that the heat transfer from the hot gas kernel is higher than the chemical heat release due to adverse effect

of $\frac{u'}{S_{b(\phi=1)}}$ (see section [2.4]) and thereby flame kernel eventually extinguishes by the time which is further explained in the next section of this chapter.

From the discussion above, it shows that the values of a_{sp} play an important role in achieving self-sustained combustion and has been chosen which ensures successful ignition and self-sustained combustion for all the cases, except for the case BR. It can also be seen that increasing $u'/S_{b(\phi=1)}$ requires more MIE and increases precipitously in BR regime since as turbulence intensity is more, in this regime turbulence eddies have high kinetic energy and they penetrate through flame reaction zone (see figure 2.1), and disturb the reaction zone which further affects the flame propagation. Mastorakos and Patel and Chakraborty [38, 45, 46] studied the flame propagation in broken reaction regimes and the present results are consistent with these literature.

4.2 Global behavior of Non-dimensional maximum temperature and turbulence decay profile

The temporal evolution of the maximum values of non-dimensional temperature (T_{max}) and corresponding turbulence decay profile are shown in figures 4.2, where effects of Ka on selected stratified and homogeneous mixtures are shown and figure 4.3, where effects of l_ϕ/l_f on combustion regime is shown respectively.

The ignition behavior of rapid increase in T_{max} for $0 < t < t_{sp}$ is common in both homogeneous and stratified mixtures. The high thermal gradient between hot gas kernel and the surrounding unburned reactant gives rise to high rate of heat transfer from the ignition kernel, which in turn leads to decrease in T_{max} once the igniter is switched off. The T_{max} approaches the non-dimensional adiabatic temperature $T \approx 1.0$ for $\phi = 1.0$ at $t > t_{sp}$, where heat release overcomes the heat transfer from the hot gas kernel and confirms self-sustained combustion is achieved. It can be seen from the figures 4.2 and 4.3 that the conditions which lead to obtain self-sustained combustion after successful ignition depend on $\frac{u'}{S_{b(\phi=1)}}$ and l_ϕ/l_f.

Additionally, figure 4.2 shows that T_{max} fails to attain the adiabatic flame temperature for the cases 24TRA, BRA and HBR, suggesting adverse effect of Ka on these cases. It is clearly seen that the probability of flame extinction at $t > t_{sp}$ increases with increasing $\frac{u'}{S_{b(\phi=1)}}$.

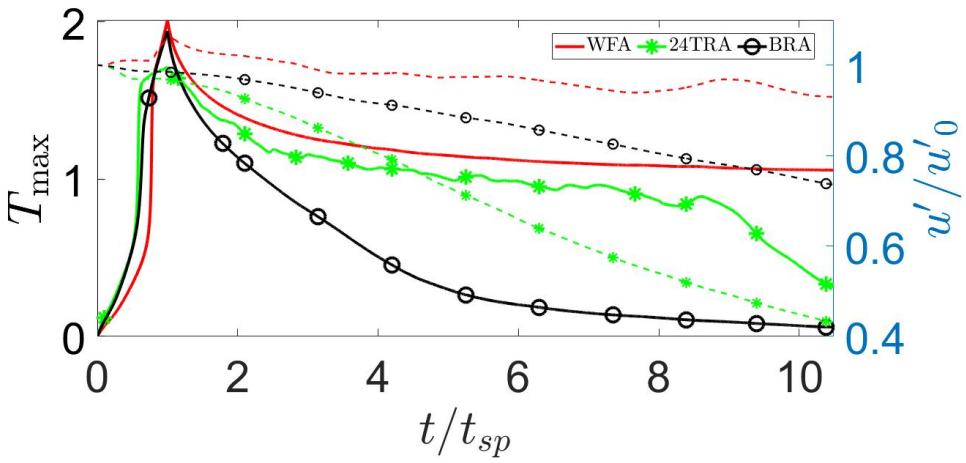

Case 1: Stratified cases

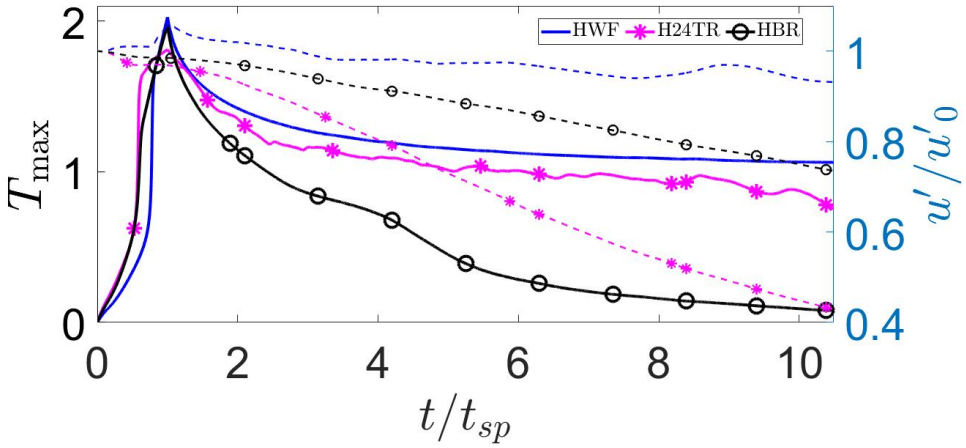

Case 2: Homogeneous cases

Figure 4.2: Temporal evolution of T_{max} and the corresponding turbulence decay profile for the selected stratified cases (top) with $l_\phi/l_f = 1.6$ and the corresponding homogeneous cases (bottom) from Table 4.1

Thereby, with the evidence seen in the figure 4.1, it suggests that the cases with $\frac{u'}{S_{b(\phi=1)}} = 41.6$ (BRA, BRB, BRC, HBR) and $\frac{u'}{S_{b(\phi=1)}} = 24$ (24TRA) may require an additional external energy after $t > t_{sp}$ in able to achieve self-sustained combustion. Figure 4.2 shows that cases WF, CF and TR with increasing Ka, the peak value of T_{max} at $t = t_{sp}$, reduces (except for case BR) for a given amount of energy deposition. From these results, it indicates that the nature of initial mixture distribution, $\frac{u'}{S_{b(\phi=1)}}$, and l_ϕ/l_f have important influences on the possibility of achieving self sustained combustion, followed by successful ignition in stratified cases.

Furthermore, it can be seen that $\frac{u'}{S_{b(\phi=1)}}$ decays for all the cases especially for high Ka number i.e. for case BR where laminar burning velocity is observed to be relatively low for given ϕ value with time (see figure 3.1), also, as the eddy thermal diffusivity which can be scaled as, $D_t \sim u' L_{11}$ decreases with time [13, 43]. The surface area to volume ratio of the hot gas kernel decreases with the expansion of the flame kernel. This along with decreasing surface to volume ratio with time leads to a reduction in the magnitude of heat transfer rate from the hot gas kernel as time progresses, which leads to more favorable condition for thermal runaway in the cases of high values of the T_{max}. Thereby, the duration over which the peak value of T_{max} is obtained after $t = t_{sp}$ also influenced by the turbulence intensity.

Figure 4.3 shows the effects of $\frac{l_\phi}{l_f}$ on temporal evolution of T_{max} and turbulence decay for $\frac{u'}{S_{b(\phi=1)}} = 24$. Moreover, it can be seen from the figure 4.3b that the influence of l_ϕ/l_f plays a major role for obtaining self-sustained combustion for all the stratified cases. The stratified cases with $\frac{u'}{S_{b(\phi=1)}} = 24$ attain successful ignition and self-sustained combustion, except for the case 24TRA showing the gradual flame extinction for the lower value of l_ϕ/l_f under the effect of high turbulence intensity, thereby shows some non-monotonic behavior for l_ϕ/l_f.

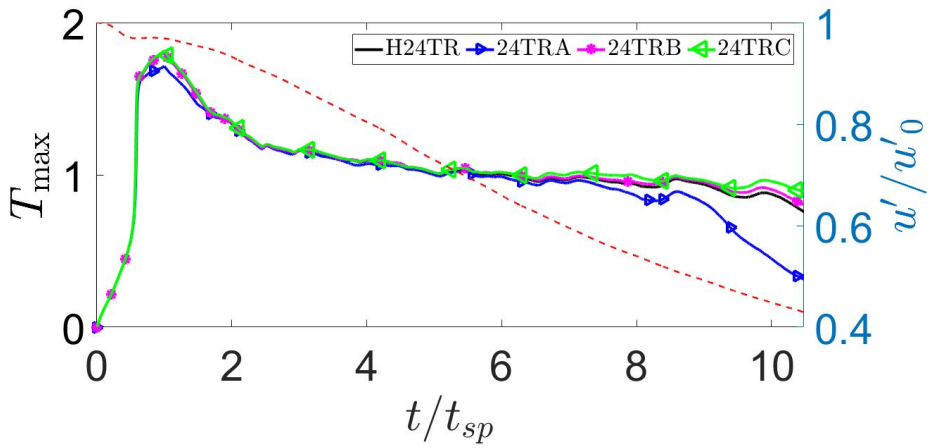

(a) case 24TR

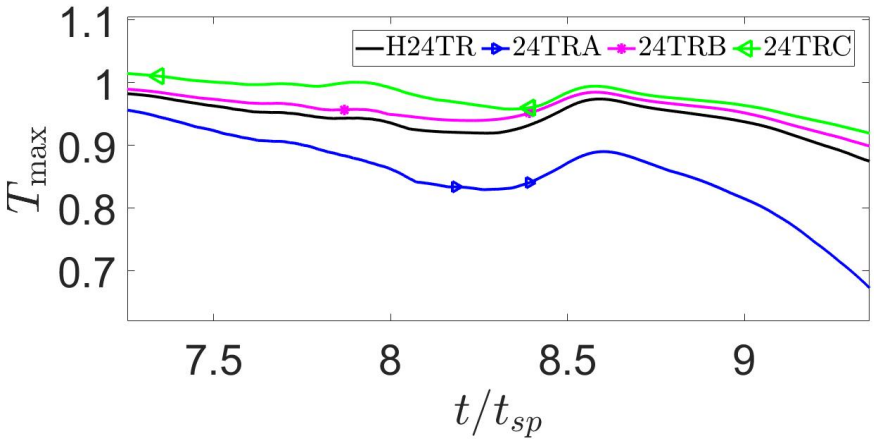

(b) Case 24TR for $7.0t_{sp} < t < 10.5t_{sp}$

Figure 4.3: Temporal evolution of T_{max} and the corresponding turbulence decay profile for the case 24TR

The above discussion propose that $\frac{u'}{S_{b(\phi=1)}}$, Ka and l_ϕ/l_f have important influence on possibility of self-sustaining combustion, after achieving successful ignition. Furthermore, the effects of l_ϕ/l_f on the success of self-sustained combustion is observed, from figure 4.3b with $l_\phi/l_f = 1.6$ are more prone to flame extinction than with the cases with $l_\phi/l_f = 2.5$ and 4.5. Moreover it is been observed in figure 4.2 that high value of temperature during ignition can be avoided for higher values of Ka i.e for 24TR as compared to case WF, which ultimately reduces thermal NO_X emission and still achieve self-sustained combustion [43].

4.3 Spatial distribution of Fuel mass fraction, Magnitude of reaction rate and Equivalence ratio

The distribution of fuel mass fraction (Y_F), magnitude of reaction rate ($\dot{\Omega}_F$) and equivalence ratio (ϕ) for the selected cases from table 4.1 at $t = 1.05t_{sp}, t = 5.78t_{sp}$ and $t = 10.5t_{sp}$ are shown in the figures [4.4 4.5],[4.6 4.7] & [4.8 4.9] respectively, where normalized magnitude of reaction rate is defined as:

$$(\dot{\Omega}_F)_{max} = (|\dot{w}_F|)_{max} \times \frac{l_f}{\rho_0 S_{b(\phi=1)}} \tag{4.3}$$

Figure 4.4 shows that the fuel mass fraction Y_F is depleted to very greater extent with increase in time steps for all the cases shown here. It is observed that the contours of Y_F are more wrinkled in TR cases as compared to WF and CF cases.

The Fuel mass fraction depletes by time in case of TR as shown in figure 4.5 due to consumption of fuel, followed by high rate of chemical reaction. In case of $\frac{u'}{S_{b(\phi=1)}} = 24$, it is observed that Y_F depletes with very high rate of chemical reaction from $t \geq 5.78t_{sp}$, followed by self-sustaining combustion.

Figure 4.6 and 4.7 represent $\dot{\Omega}_F$ for the selected cases from table 4.1. WF and CF cases (figure 4.6) propound to show high amount of reaction rate with expansion of temperature (see figure 4.11) by the time. It is observed that $\dot{\Omega}_F$ for the case 24TR gets wrinkled and eventually decreases by the time due to consumption of fuel.

Moreover, figures 4.8 and 4.9 represent the distribution of equivalence ratio (ϕ) and is noticed that the non-uniformity of ϕ decreases with the time interval in all the cases suggesting a good rate of mixing. It can been seen that the distribution of inhomogeneity broadens, with increase in $\frac{l_\phi}{l_f}$. Furthermore, figure 4.9 shows that $\frac{l_\phi}{l_f} = 1.6$, associate more with fuel rich mixture, whereas $\frac{l_\phi}{l_f} = 4.5$ represent fuel lean.

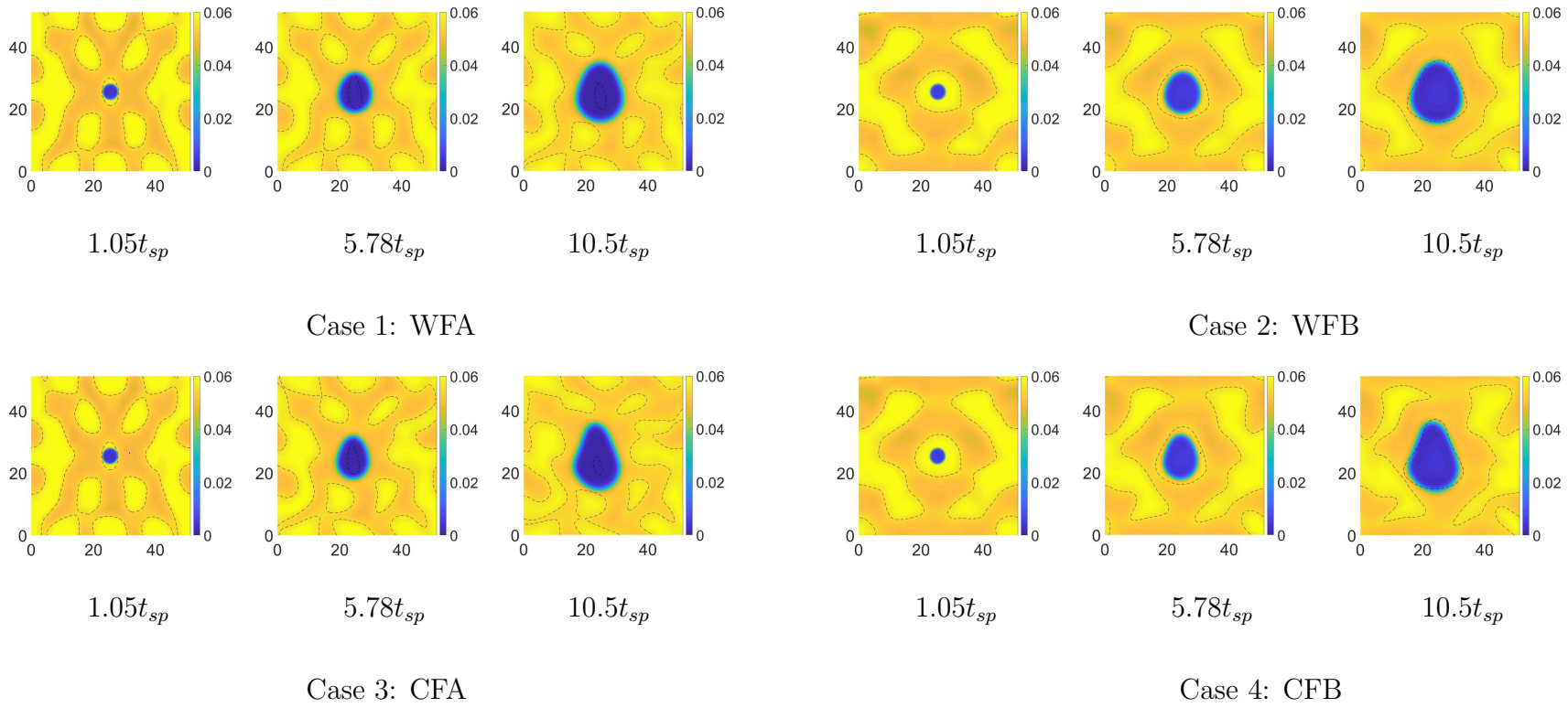

Figure 4.4: Distribution of Fuel mass fraction (Y_F) within the cubic domain of $51l_f \times 51l_f \times 51l_f$ for the cases WF (1^{st} row) and CF (2^{nd} row)

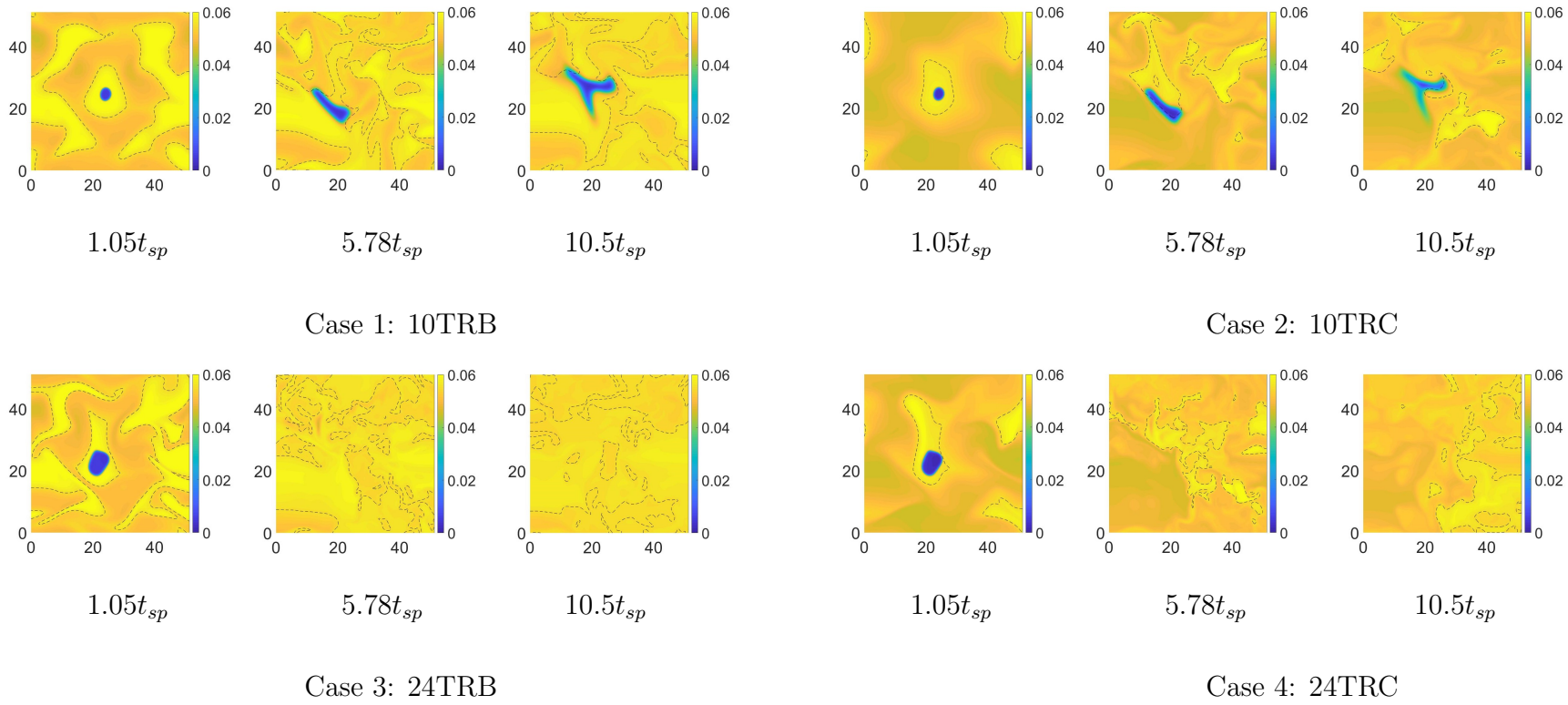

Figure 4.5: Distribution of Fuel mass fraction (Y_F) within the cubic domain of $51l_f \times 51l_f \times 51l_f$ for the cases 10TR (1^{st} row) and 24TR (2^{nd} row)

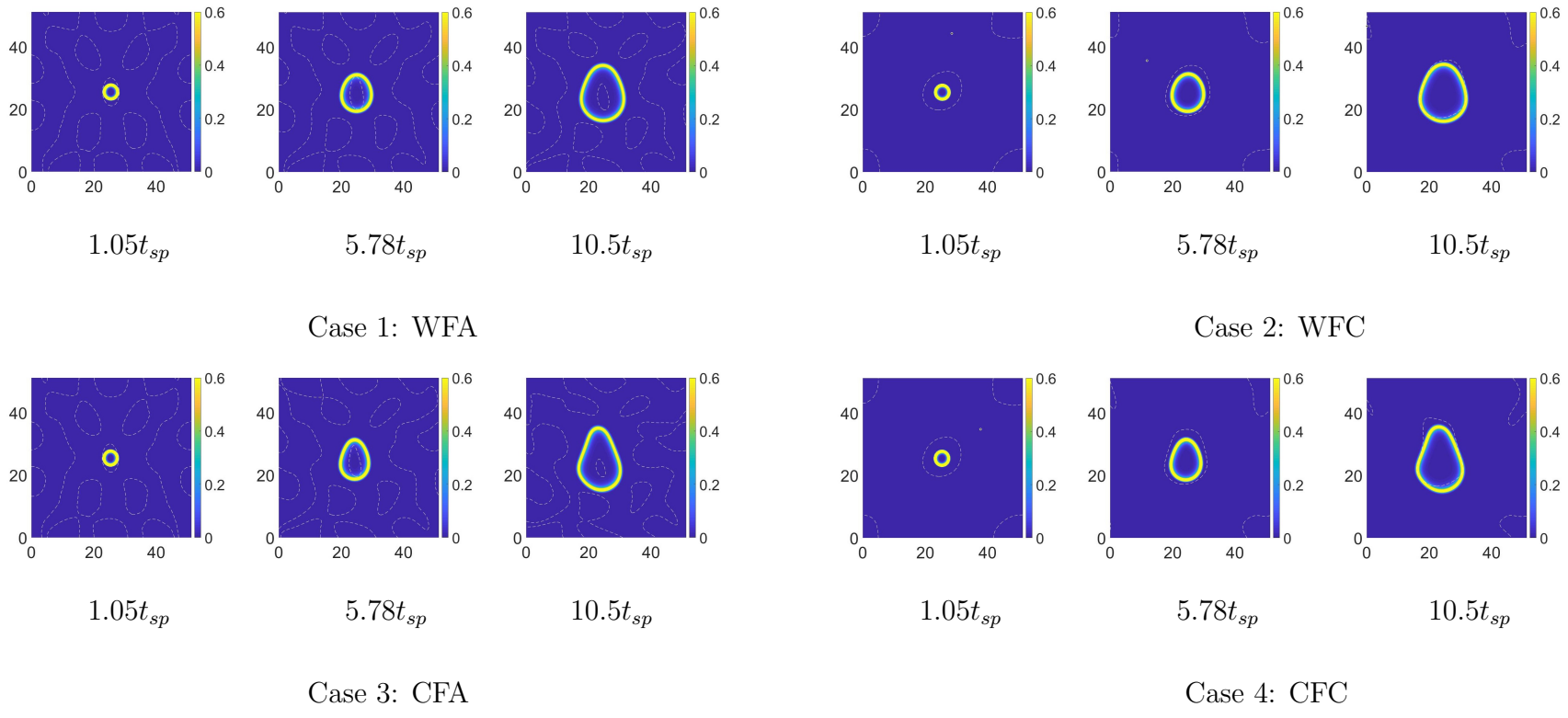

Figure 4.6: Distribution of Reaction rate ($\dot{\Omega}_F$) within the cubic domain of $51l_f \times 51l_f \times 51l_f$ for the cases WF (1^{st} row) and CF (2^{nd} row)

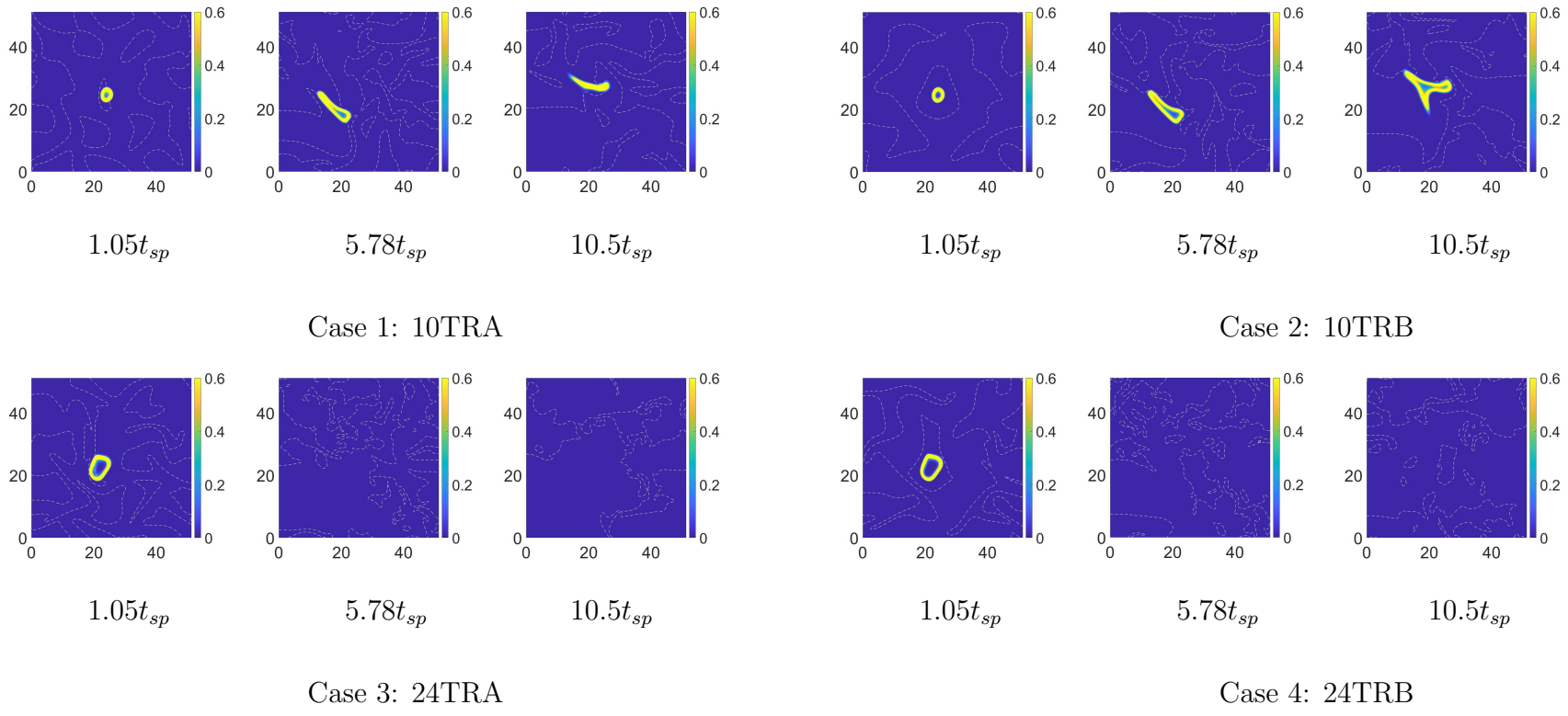

Figure 4.7: Distribution of Reaction rate ($\dot{\Omega}_F$) within the cubic domain of $51l_f \times 51l_f \times 51l_f$ for the cases 10TR (1^{st} row) and 24TR (2^{nd} row)

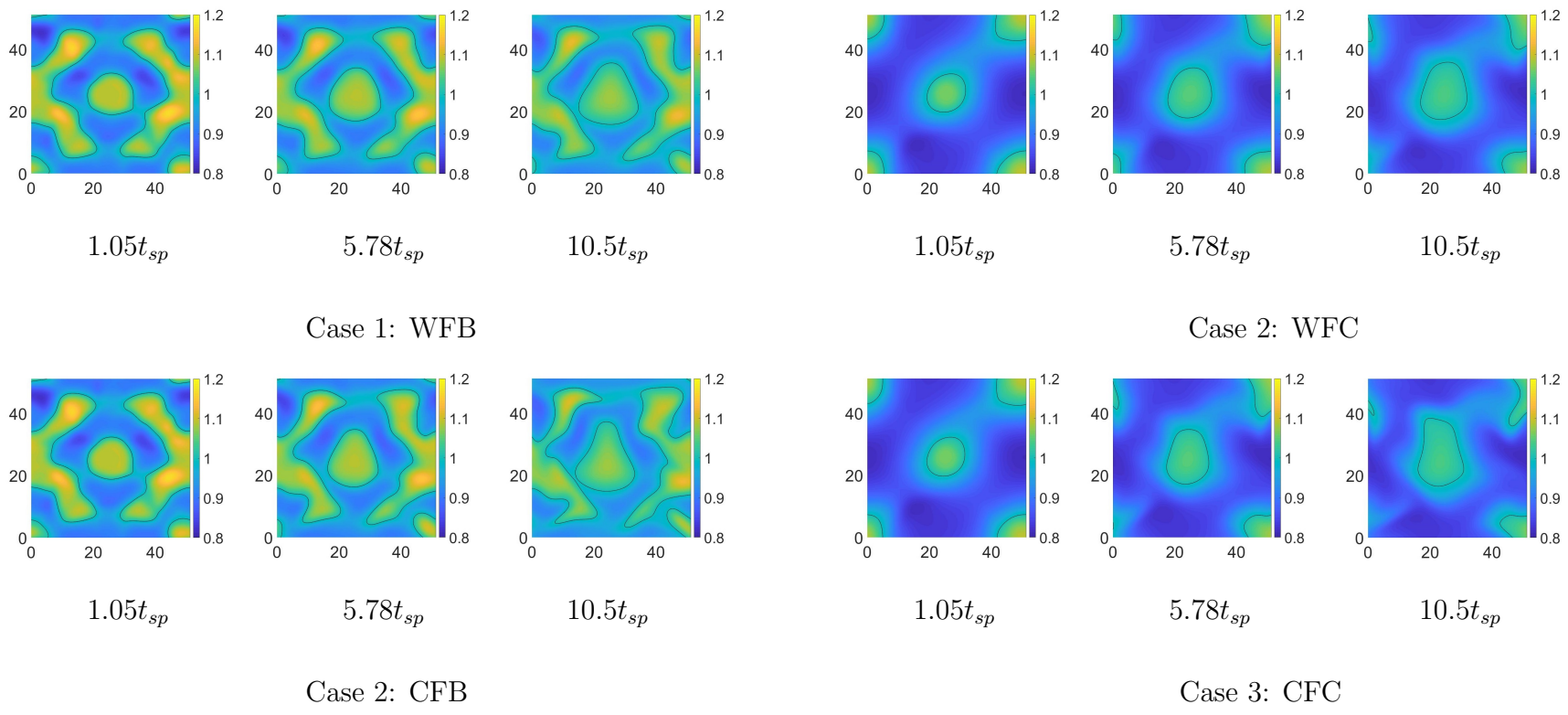

Figure 4.8: Distribution of Equivalence ratio (ϕ) within the cubic domain of $51l_f \times 51l_f \times 51l_f$ for the cases WF (1^{st} row) and CF (2^{nd} row)

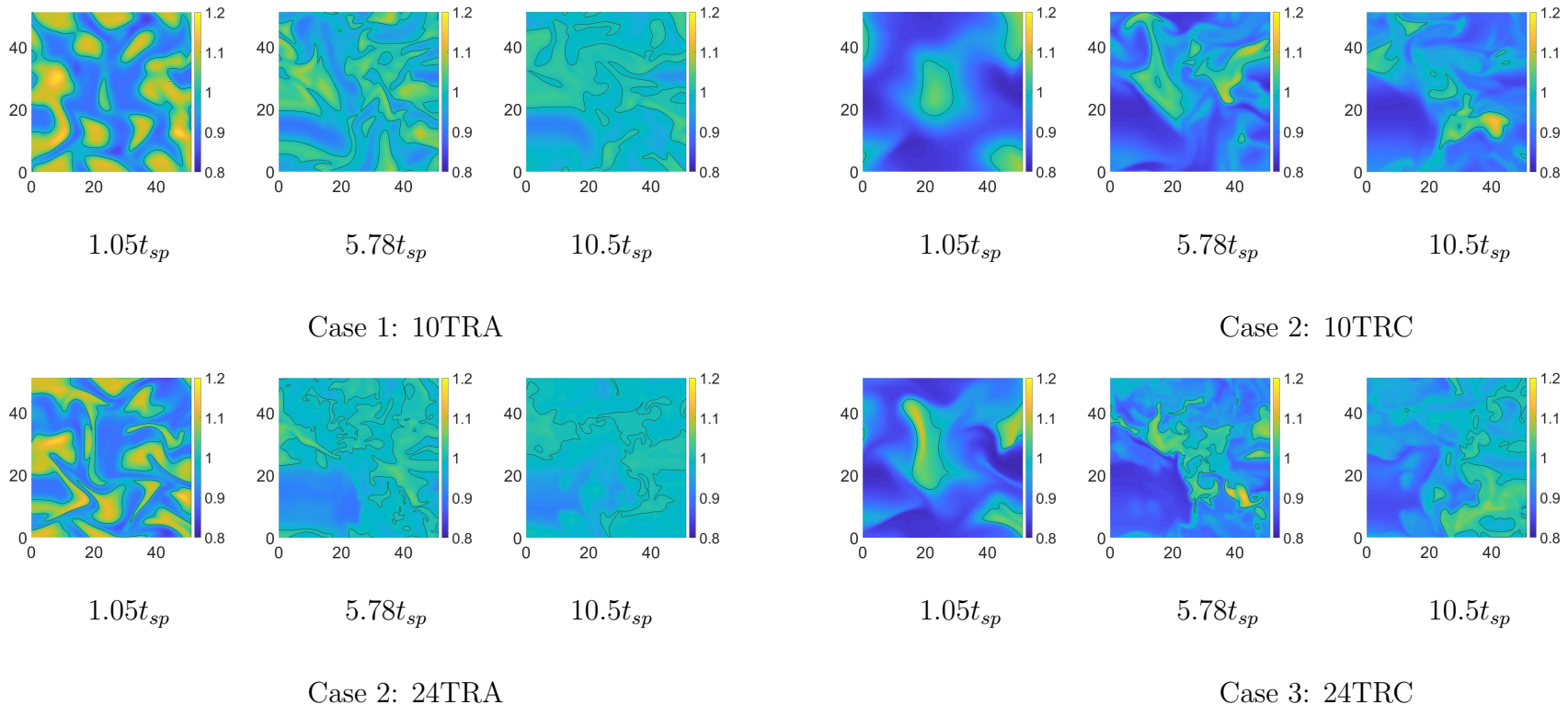

Figure 4.9: Distribution of Equivalence ratio (ϕ) within the cubic domain of $51l_f \times 51l_f \times 51l_f$ for the cases 10TR (1^{st} row) and 24TR (2^{nd} row)

4.4 Flame - Turbulence interaction

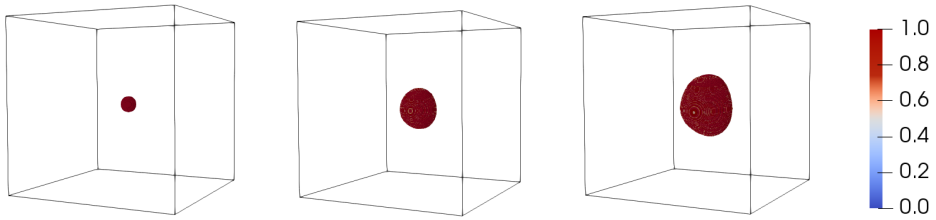

Case 1: WFA

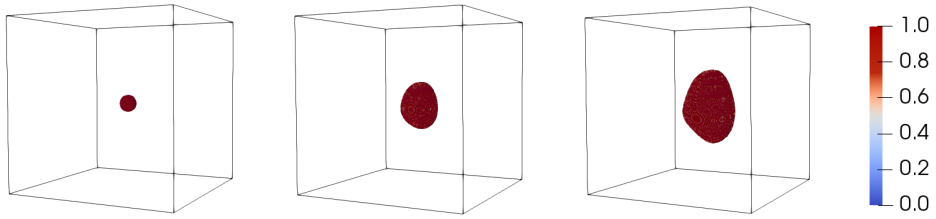

Case 2: CFB

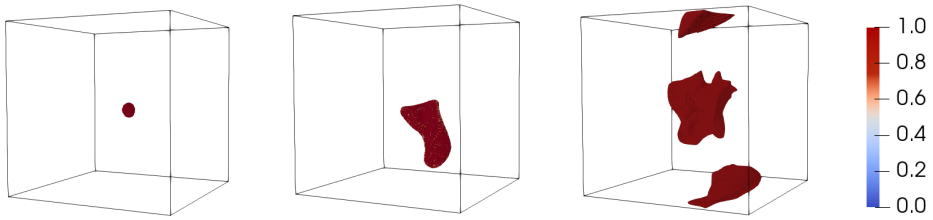

Case 3: 10TRC

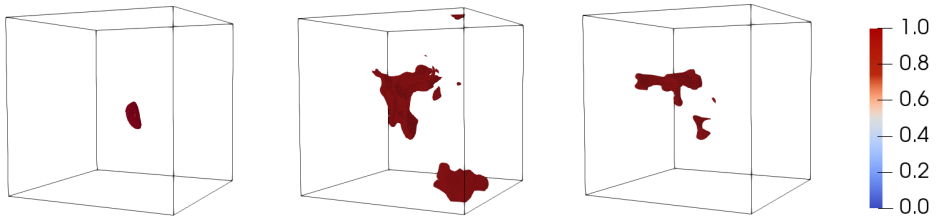

Case 4: 24TRA

Figure 4.10: Non-dimensional temperature profile within the simulation domain for the selected stratified cases from the Table 4.1 at $1.05_{tsp}(1^{st}$ column), $5.78_{tsp}(2^{nd}$ column), & $10.5_{tsp}(3^{rd}$ column)

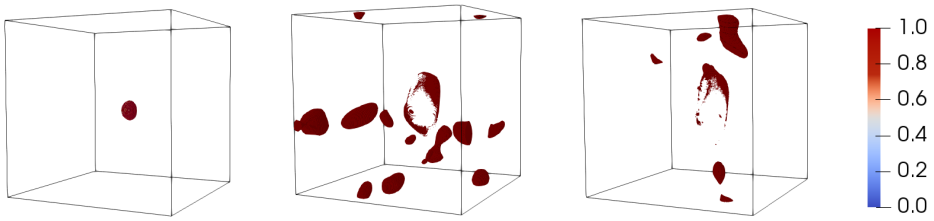

Case 1: BRA

Figure 4.11: Non-dimensional temperature profile within the simulation domain for the broken reaction ($u'/S_{b(\phi)} = 41.6$) at $1.05_{tsp}(1^{st}$ column), $2.1_{tsp}(2^{nd}$ column) & $2.63_{tsp}(3^{rd}$ column)

The distribution of temperature (T) profile within the simulation domain for the selected cases from table 4.1 are shown in figures 4.10 and 4.11. It can be seen that the profile of T remain approximately circular during the period of energy deposition ($t \leq t_{sp}$) but they become increasingly wrinkled as time progresses. Turbulence intensity show significant effect on the development of flame kernel (figure 4.10). The extent of temperature for a mixture composition depends on diffusion of energy deposition before the ignition, and then depends on turbulence intensity with magnitude of reaction rate after the ignition phase [43, 44] and is been observed in figure 4.10.

Due to low turbulence level of $\frac{u'}{S_{b(\phi=1)}} = 0.8$ and $\frac{u'}{S_{b(\phi=1)}} = 1.5$ (WF & CF), the temperature profile remains spherical over the entire simulation duration till $10.5t_{sp}$ (see figure 4.10). For the TR cases, the flame kernel is been distressed by high turbulence effect. The temperature profile for the case 24TRA gets lower with time, eventually fails to attain self-sustained combustion (observed to be consistent with figure 4.3a). In case of TR, the hot gas kernel increasingly corrugates from spherical shape due to high turbulence intensity, where the energetic eddies penetrate into the reaction zone and fragment them at $t \gg t_{sp}$. Thereby, the hot gas kernel becomes completely distorted at the end of simulation for the cases 10TRC and 24TRA.

Similarly with the case BR, it can be seen that the temperature profile gets distorted by the time interval and gradually vanishes by time, exhibiting that self-sustained combustion is not achieved (also seen in figure 4.2).

The development of flame kernel depends on the heat release due to chemical reaction and the heat transfer from the hot gas kernel. Thereby, it shows that at high temperature region where chemical reaction takes place has been fragmented in the case 24TR and BR at $t \gg t_{sp}$ due to penetration of energetic eddies into the preheat zone of flame. This fragmented high temperature region is indicative of disturbance of the reaction zone by turbulence under high values of Ka.

4.5 Mixing Statistics

Probability density function (PDF) of the equivalence ratio specifies the probability of ϕ falling within a particular range of mixture composition. The evolution of mixing process is been shown in figures 4.12 and 4.13 by temporal evolution of PDF of ϕ.

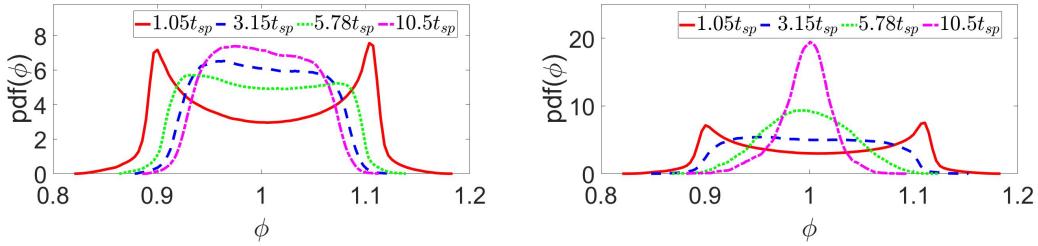

Figure 4.12: Temporal evolution of the PDF of ϕ for the cases WFA (left) and 10TRA (right) at $t = 1.05_{tsp}$, $t = 3.15_{tsp}$, $t = 5.78_{tsp}$, & $t = 10.5_{tsp}$

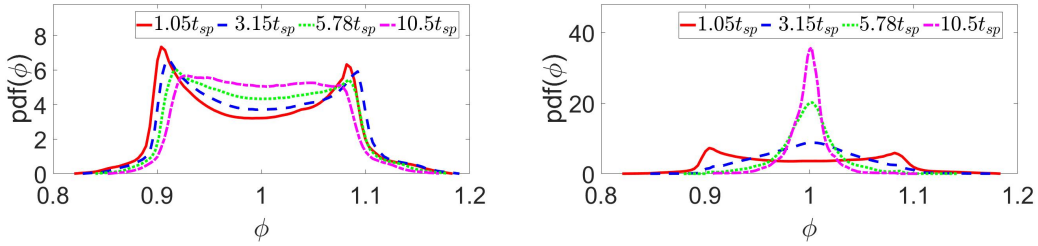

Figure 4.13: Temporal evolution of the PDF of ϕ for the cases CFB (left) and 24TRB (right) at $t = 1.05_{tsp}$, $t = 3.15_{tsp}$, $t = 5.78_{tsp}$ & $t = 10.5_{tsp}$

It is observed from the figure 4.12 and figure 4.13 that for the low Ka (i.e low turbulence intensity), cases WF and CF remains Bi-modal even at $t = 10.5t_{sp}$ with initial Bi-modal distribution of ϕ (also seen in figure 4.8). For the cases 10TR and 24TR, the PDF of ϕ approach Gaussian profile with peak $\phi \approx \langle\phi\rangle$, with decrease in ϕ' as the time increases. This results in achieving stoichiometric level of mixture, i.e $\phi \approx \langle\phi\rangle$. The case 10TRA results to Gaussian profile from $t \geq 5.78t_{sp}$, shown in the figure 4.12 and the case 24TRB draws the same outcome at $t \geq 3.15t_{sp}$ as shown in figure 4.13. Also, it is been observed that mixing process is slower for higher values of l_ϕ/l_f and Ka.

4.6 Effects of l_ϕ/l_f and Ka on the Extent of Burning

The degree of chemical reaction can be presented in terms of reaction variable c, which is defined as [43–45]:

$$c = \frac{Y_{Fu} - Y_F}{Y_{Fu} - Y_{Fb}} \tag{4.4}$$

In case of stratified mixtures, [45]

$$c = \frac{\xi Y_{F\infty} - Y_F}{\xi Y_{F\infty} - \max\left[0, \frac{\xi - \xi_{st}}{1 - \xi_{st}}\right] Y_{F\infty}} \tag{4.5}$$

The extent of burning can be characterized by normalized burned gas mass with $c \geq 0.9$ and is defined as [43] [21]:

$$M_b = \frac{m_b(c \geq 0.9)}{\frac{4}{3}\pi\rho_0 l_f^3} \tag{4.6}$$

The term $\frac{4}{3}\pi\rho_0 l_f^3$ represent volume mass of an unburned gas sphere. The burned gas mass in the above equation 4.5 is normalized by volume mass of unburned gas in

a sphere with radius equal to Zel-dovich flame thickness l_f [59]. Figure 4.14 and 4.15 represent the temporal evolution of burned gas mass for all the cases from Table 4.1.

Figure 4.14 shows the effects of l_ϕ/l_f on the extent of burning. It demonstrates that the initial value of $\frac{l_\phi}{l_f}$= 2.5 and 4.5 shows higher value of M_b than $\frac{l_\phi}{l_f}$= 1.6 for the given mixture. As seen in the figure 4.8 and 4.9, the clouds of mixture inhomogeneity increases with increase in $\frac{l_\phi}{l_f}$ value and thereby, the igniter may have exist in a larger region of homogeneous mixture, thereby results in high rate of burning for higher values of $\frac{l_\phi}{l_f}$. If the igniter is present in large clouds of $1.0 \leq \phi \leq 1.2$, the mixture will accelerate the expansion of hot gas kernel and thus increases the burning rate. Mixing rate for the case $\frac{l_\phi}{l_f}$= 2.5 shows that it leads to attain more M_b than $\frac{l_\phi}{l_f}$= 4.5. Value of M_b is observed to be maximum for $\frac{l_\phi}{l_f}$= 2.5 for respective value of $\frac{u'}{S_{b(\phi=1)}}$. It is observed that the case BR fails to attain self-sustained combustion despite of successful ignition. From section 4.2, it is observed that the heat loss overcomes the chemical heat release and thereby hot gas kernel shrinks and heat release drops continuously leading to flame extinction which is also been seen in section 4.4 figure 4.11. It is seen that M_b varnishes after $t = 3t_{sp}$. Also, figure 4.14 shows that M_b for all the stratified cases attains higher value than the respective homogeneous cases (except for the case BR) suggesting better option towards positive results.

The eddy thermal diffusivity in turbulent flow scale can be scaled as [43]:

$$D_t \sim u' L_{11} \tag{4.7}$$

The above equation shows that the increase in u' for given value of L_{11} will enhance the rate of heat transfer from the hot gas kernel. Figure 4.15 shows that increase in $\frac{u'}{S_{b(\phi=1)}}$ (observed to be consistent for all l_ϕ/l_f values) reduces the extent of burning. Case WF shows to attain the highest value of M_b. It is been observed in section 4.2 figure 4.2 that increase in $\frac{u'}{S_{b(\phi=1)}}$increases the eddy thermal diffusivity, leading to inconsistent preheat zone with flame structure which further leads to reduction of

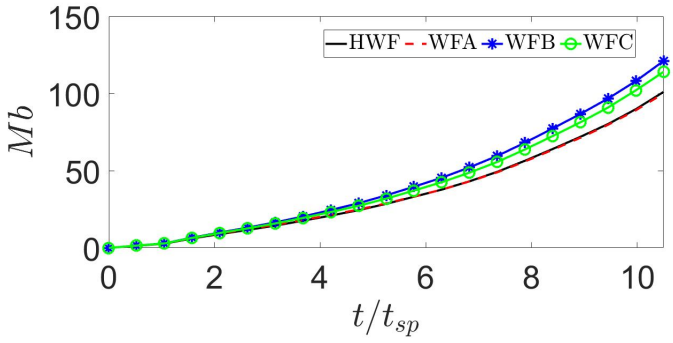

Case 1: WF

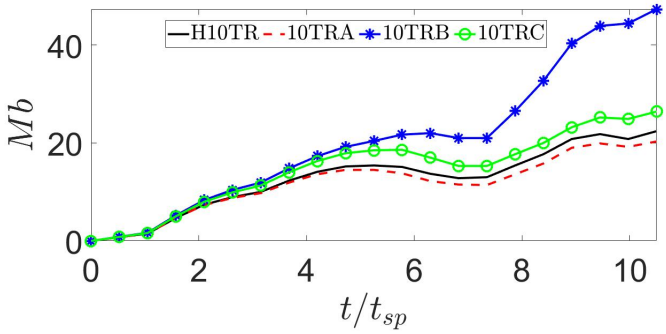

Case 2: 10TR

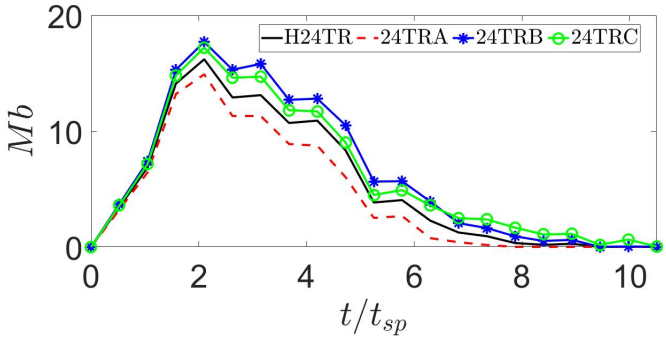

Case 3: 24TR

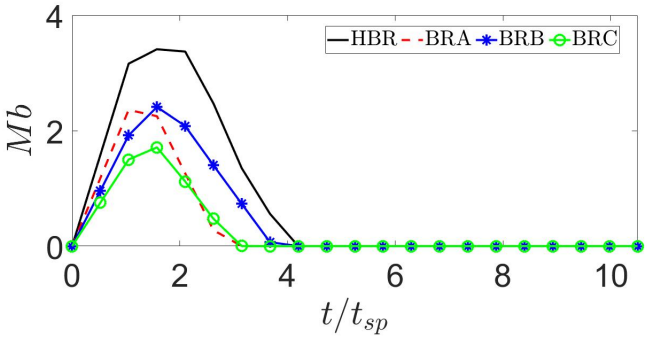

Case 4: BR

Figure 4.14: Temporal evolution of M_b for all the cases listed in Table 4.1

flame kernel surface area and reduction of burned gas mass. In the case of 10TR, it is observed that heat transfer overcomes the chemical heat release at early stages of flame evolution, which gives rise to a reduction of M_b for the time interval of $5.5t_{sp} < t < 7.5t_{sp}$, similarly it is observed in case 24TR, that the value of M_b gradually decreases after $2.0t_{sp}$. At $t = 8.0t_{sp}$ (case 10TR), it is seen that the rate of heat transfer reduces with time and the chemical heat release starts to exceed the heat transfer rate from the hot gas kernel which increases M_b with time again. In case of BR, the hot gas kernel is shrinking in contradiction and eventually the flame vanishes once the heat transfer overcomes the chemical heat release showing no burning rate.

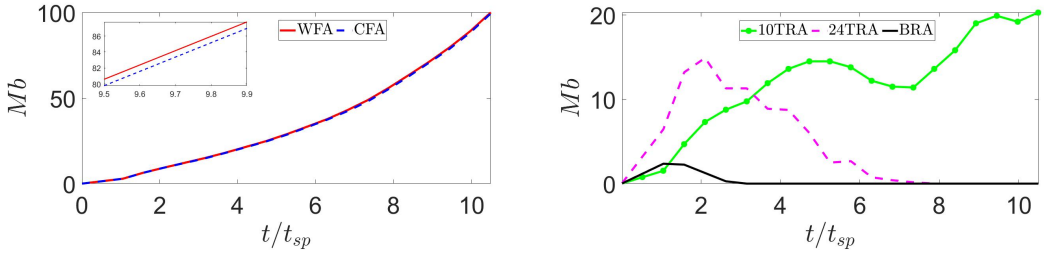

Figure 4.15: Temporal evolution of M_b for the selected stratified cases from the Table 4.1

The results from the figures 4.14 and 4.15 suggests that the degree of burning depends on combustion regimes with values of $\frac{u'}{S_{b(\phi=1)}}$, l_ϕ/l_f and nature of mixture distribution. It has been observed that increase in turbulence intensity reduces the extent of burning, augmenting the rate of heat transfer from the hot gas kernel and thereby possible to attain flame extinction. The detrimental effects of $\frac{u'}{S_{b(\phi=1)}}$ on ignition and early stages of burning are observed for higher values of Ka due to increase of eddy diffusivity with increase in turbulence intensity which results in volume reduction of the flame kernel thereby reducing the burning rate. This results are found consistent with previous experimental studies [5, 27, 35] and computational results [10–12, 22, 43, 44] findings.

Chapter 5

Conclusions and Future work

5.1 Conclusions

All the simulations in this thesis are performed using three- dimensional compressible DNS code SENGA. Effects of turbulent combustion regimes on localized forced ignition have been investigated and key observations and findings are presented in this chapter.

The effects of Karlovitz number (Ka) and energy deposition (a_{sp}) characteristics on MIE requirements for successful ignition and self-sustained combustion have been investigated in section 4.1. Increase in Ka increases the requirements of MIE to achieve self-sustained combustion and it is observed that it increases abruptly for the case BR. Also, it has been seen that the value of a_{sp} plays an important role to achieve successful ignition and self-sustained combustion in both homogeneous and stratified mixture. Based on the current findings, one can choose spark plug energy deposition value which not only grantees the ignition but also confirms self sustained combustion. Moreover, figure 4.1 shows that the MIE value lower than the favorable value leads to unsuccessful ignition and increasing beyond the optimal value increases the value of T_{max} redundantly leading to increase in NO_X emissions which is also in good agreement with previous studies [9, 45, 46]. It is proposed that $\frac{u'}{S_{b(\phi=1)}}$, $\frac{l_\phi}{l_f}$

and ϕ have important influence on possibility of attaining self-sustained combustion, ensuing with successful ignition.

The fuel mass fraction (Y_F) depletes to very greater extent with increase in time simulation. The magnitude of reaction rate ($\dot{\Omega}_F$) corrugates with the expansion of time due to consumption of fuel. Moreover, it is noticed that the non-uniformity of ϕ for the case TR decreases by time in all the cases, resulting in change from mixture inhomogeneity to homogeneous mixture i.e $\phi \approx \langle\phi\rangle$.

The temperature profile is observed to attain spherical profile during the energy deposition corrugates for the TR and BR cases as the time progresses. The extent of temperature for the cases 24TRA and BR gets lower with time, due to penetration of energetic eddies into reaction zone of flame kernel which leads to the high temperature between hot gas kernel and the surrounding unburned reactant, rising to high rate of heat transfer from the ignition kernel which eventually fails to attain self-sustained combustion. The mixing process is slower for higher values of l_ϕ/l_f for all cases and the width of PDF of ϕ decreases with time.

The rate of burning is observed to be higher in stratified cases than the corresponding homogeneous cases (see figure 4.14). Case WF shows to attain the highest value of M_b as compared to rest of the cases. Figure 4.14 shows that the value of M_b is observed to be maximum for $l_\phi/l_f = 2.5$ (non-monotonic behavior) for corresponding value of $\frac{u'}{S_{b(\phi=1)}}$ due to the location of the igniter in the proximity of the fuel-rich mixture. The rate of burning decreases with increase in $\frac{u'}{S_{b(\phi=1)}}$ which shows possibility of flame extinction. The results obtained suggests that the degree of burning depends on values of $\frac{u'}{S_{b(\phi=1)}}$, l_ϕ/l_f and nature of mixture distribution. The variability of burned gas mass is obtained in the cylinder of IC engines due to cycle-to-cycle variation [43].

The degree of burning depends on all the parameters, including the nature of initial mixture distribution. This can be adjusted by careful design of the fuel injector nozzle in IC engines. In-cylinder fuel injector provides benefits over conventional

carburetor system, where fuel injector nozzle can be carefully designed to provide consistent fuel distribution where the fuel will mix with existing air to form stratified mixture. And the overall mixture will provide prescribed distribution of ϕ to take advantages of stratified mixture. Moreover, in-cylinder turbulence along with injection characteristics can influence the values of $\frac{u'}{S_{b(\phi=1)}}$, l_ϕ/l_f , and thereby the control of mixing characteristics in IC engine combustion chamber can potentially play a pivotal role to ensure successful ignition and reduce the variability on M_b associated with the ignition event [43]. The computational findings in this study has been found consistent with the previous experimental findings [5, 27, 35].

It is possible to obtain successful ignition and self-sustained combustion for all the stratified cases (including BR cases) by judicious choice of R, b_{sp}, a_{sp} and these parameters can be altered independently of each other in case of laser ignition. The present findings are consistent with recent experimental findings [14] that laser ignition can be effective in igniting stratified mixtures by altering the laser power (i.e. equivalent to the variation of a_{sp}), laser beam radius (i.e. equivalent to the variation of R) and pulse durations (i.e. equivalent to the variation of bsp). The present results shows advantages of stratified mixture over homogeneous for achieving higher burning rate. This suggests that SCCI (stratified Charge Compression Ignition) have more potential for diesel-like efficiencies and very low emission of NO_X and particulate [32, 33].

5.1.1 Limitations in current study

- The present study shows results for only given realization of ϕ. Further study of different realization of ϕ and different distribution (e.g Gaussian) is required to investigate cycle-to-cycle variation experiencing in IC engines.

- The present study shows results by adapting single step Arrhenius type chemistry. Further investigation is required for detailed chemistry with higher turbulent Reynolds number.

- In order to keep the current study computationally feasible, the shock and plasma waves originated by the igniter has not been considered here.

5.2 Future work

The presented study shows physical understanding of various aspects involved in localized forced ignition of turbulent stratified and homogeneous mixtures. For further investigation of the forced ignition of combustible mixtures, following study can be considered:

- Effects of different distribution (from Gaussian profile) on higher value of Ka.

- Effects of Fuel Lewis Number greater than unity, on localized forced ignition.

- Effects of complex chemistry, of industrially relevant fuels for higher number of Re_t.

- Effects of successful ignition and subsequent self-sustained combustion processes in development of HCCI engines.

Bibliography

[1] Thoughtco: What is compression ignition, the starting power of diesel engines. `https://www.thoughtco.com/what-is-compression-ignition-85351`. Accessed: 2019.

[2] S. K. Aggarwal. A review of spray ignition phenomena: present status and future research. *Progress in Energy and Combustion Science*, 24(6):565–600, 1998.

[3] S. Ahmed and E. Mastorakos. Correlation of spark ignition with the local instantaneous mixture fraction in a turbulent nonpremixed methane jet. *Combustion Science and Technology*, 182(9):1360–1368, 2010.

[4] A. Bakker. Lecture 10-turbulence models applied computational fluid dynamics. *Power-Point presentation*, 2002.

[5] D. Ballal and A. Lefebvre. Ignition and flame quenching of flowing heterogeneous fuel-air mixtures. *Combustion and Flame*, 35:155–168, 1979.

[6] G. K. Batchelor and A. A. Townsend. Decay of turbulence in the final period. *Proceedings of the Royal Society of London. Series A. Mathematical and Physical Sciences*, 194(1039):527–543, 1948.

[7] R. Bilger, S. Pope, K. Bray, and J. Driscoll. Paradigms in turbulent combustion research. *Proceedings of the Combustion Institute*, 30(1):21–42, 2005.

[8] H. Burchard. *Applied turbulence modelling in marine waters*, volume 100. Springer Science & Business Media, 2002.

[9] R. Cant and E. Mastorakos. *An introduction to turbulent reacting flows*. Imperial College Press, 2008.

[10] C. Catlin, M. Fairweather, and S. Ibrahim. Predictions of turbulent, premixed flame propagation in explosion tubes. *Combustion and Flame*, 102(1-2):115–128, 1995.

[11] N. Chakraborty, H. Hesse, and E. Mastorakos. Effects of fuel lewis number on localised forced ignition of turbulent mixing layers. *Flow, turbulence and combustion*, 84(1):125, 2010.

[12] N. Chakraborty and E. Mastorakos. Direct numerical simulations of localised forced ignition in turbulent mixing layers: the effects of mixture fraction and its gradient. *Flow, Turbulence and Combustion*, 80(2):155–186, 2008.

[13] N. CHAKRABORTY, E. Mastorakos, and R. Cant. Effects of turbulence on spark ignition in inhomogeneous mixtures: a direct numerical simulation (dns) study. *Combustion science and technology*, 179(1-2):293–317, 2007.

[14] G. Dearden and T. Shenton. Laser ignited engines: progress, challenges and prospects. *Optics express*, 21(106):A1113–A1125, 2013.

[15] C. Duwig and C. Fureby. Large eddy simulation of unsteady lean stratified premixed combustion. *Combustion and Flame*, 151(1-2):85–103, 2007.

[16] T. Echekki and H. Kolera-Gokula. A regime diagram for premixed flame kernel-vortex interactions. *Physics of Fluids*, 19(4):043604, 2007.

[17] F. Egolfopoulos, P. Cho, and C. Law. Laminar flame speeds of methane-air mixtures under reduced and elevated pressures. *Combustion and flame*, 76(3-4):375–391, 1989.

[18] T. Ellison and J. Turner. Turbulent entrainment in stratified flows. *Journal of Fluid Mechanics*, 6(3):423–448, 1959.

[19] T. Endo, K. Kuwamoto, W. Kim, T. Johzaki, D. Shimokuri, and S.-i. Namba. Comparative study of laser ignition and spark-plug ignition in high-speed flows. *Combustion and Flame*, 191:408–416, 2018.

[20] V. Eswaran and S. Pope. Direct numerical simulations of the turbulent mixing of a passive scalar. *The Physics of fluids*, 31(3):506–520, 1988.

[21] E. Fernandez-Tarrazo, A. L. Sánchez, A. Linan, and F. A. Williams. A simple one-step chemistry model for partially premixed hydrocarbon combustion. *Combustion and Flame*, 147(1-2):32–38, 2006.

[22] A. Frendi and M. Sibulkin. Dependence of minimum ignition energy on ignition parameters. *Combustion science and technology*, 73(1-3):395–413, 1990.

[23] K. Hanjalić and B. E. Launder. Contribution towards a reynolds-stress closure for low-reynolds-number turbulence. *Journal of Fluid Mechanics*, 74(4):593–610, 1976.

[24] D. Haworth, R. Blint, B. Cuenot, and T. Poinsot. Numerical simulation of turbulent propane–air combustion with nonhomogeneous reactants. *Combustion and Flame*, 121(3):395–417, 2000.

[25] C. Heeger, B. Böhm, S. Ahmed, R. Gordon, I. Boxx, W. Meier, A. Dreizler, and E. Mastorakos. Statistics of relative and absolute velocities of turbulent non-premixed edge flames following spark ignition. *Proceedings of the Combustion Institute*, 32(2):2957–2964, 2009.

[26] H. Hoffmeyer. *Combustion Characteristics of Turbo Charged DISI-engines*. Logos Verlag Berlin GmbH, 2012.

[27] C. Huang, S. Shy, C. Liu, and Y. Yan. A transition on minimum ignition energy for lean turbulent methane combustion in flamelet and distributed regimes. *Proceedings of the Combustion Institute*, 31(1):1401–1409, 2007.

[28] C. Jiménez, B. Cuenot, T. Poinsot, and D. Haworth. Numerical simulation and modeling for lean stratified propane-air flames. *Combustion and Flame*, 128(1-2):1–21, 2002.

[29] M. Klein, N. Chakraborty, and R. Cant. Effects of turbulence on self-sustained combustion in premixed flame kernels: a direct numerical simulation (dns) study. *Flow, turbulence and combustion*, 81(4):583–607, 2008.

[30] K. Kuo. *Principles of combustion*. A Wiley-Interscience publication. Wiley, 1986.

[31] K. K.-y. Kuo and R. Acharya. *Fundamentals of turbulent and multiphase combustion*. John Wiley & Sons, 2012.

[32] C. Lee and K. Lee. An experimental study on the combustion and emission characteristics of a stratified charge compression ignition (scci) engine. *Energy & fuels*, 21(4):1901–1907, 2007.

[33] C. Lee, E. Tomita, and K. Lee. Characteristics of combustion stability and emission in scci and cai combustion based on direct-injection gasoline engine. Technical report, SAE Technical Paper, 2007.

[34] A. H. Lefebvre. The role of fuel preparation in low emissions combustion. In *ASME 1995 International Gas Turbine and Aeroengine Congress and Exposition*, pages V005T17A001–V005T17A001. American Society of Mechanical Engineers, 1995.

[35] A. H. Lefebvre. *Gas turbine combustion*. CRC press, 1998.

[36] S. P. Malkeson and N. Chakraborty. Statistical analysis of scalar dissipation rate transport in turbulent partially premixed flames: a direct numerical simulation study. *Flow, Turbulence and Combustion*, 86(1):1–44, 2011.

[37] E. Mastorakos. Ignition of turbulent non-premixed flames. *Progress in Energy and Combustion Science*, 35(1):57–97, 2009.

[38] E. Mastorakos. Forced ignition of turbulent spray flames. *Proceedings of the Combustion Institute*, 36(2):2367–2383, 2017.

[39] S. McAllister, J.-Y. Chen, and A. C. Fernandez-Pello. *Fundamentals of combustion processes*. Springer, 2011.

[40] M. Nalim. Preliminary assessment of combustion modes for internal combustion wave rotors. In *31st Joint Propulsion Conference and Exhibit*, page 2801, 1995.

[41] A. Neophytou, E. Mastorakos, and R. Cant. Dns of spark ignition and edge flame propagation in turbulent droplet-laden mixing layers. *Combustion and Flame*, 157(6):1071–1086, 2010.

[42] N. Pasquier, B. Lecordier, M. Trinite, and A. Cessou. An experimental investigation of flame propagation through a turbulent stratified mixture. *Proceedings of the Combustion Institute*, 31(1):1567–1574, 2007.

[43] D. Patel. *Fundamental investigation of localised forced ignition in turbulent homogeneous and stratified mixtures*. PhD thesis, Newcastle University, 2017.

[44] D. Patel and N. Chakraborty. Localised forced ignition of globally stoichiometric stratified mixtures: A numerical investigation. *Combustion Theory and Modelling*, 18(6):627–651, 2014.

[45] D. Patel and N. Chakraborty. Effects of mixture distribution on localised forced ignition of stratified mixtures: A numerical investigation. In *25th International Colloquium on Dynamics of Explosions and Reactive Systems*. Newcastle University, 2015.

[46] D. Patel and N. Chakraborty. Effects of fuel lewis number on localised forced ignition of turbulent homogeneous mixtures: A numerical investigation. *International Journal of Spray and Combustion Dynamics*, 8(3):183–196, 2016.

[47] H. Pearlman and R. M. Chapek. Cool flames and autoignition: thermal-ignition theory of combustion experimentally validated in microgravity. 2000.

[48] N. Peters. Four lectures on turbulent combustion. *ERCOFTAC Summer School*, 1997.

[49] N. Peters. *Turbulent combustion*. Cambridge university press, 2000.

[50] T. X. Phuoc. Laser-induced spark ignition fundamental and applications. *Optics and Lasers in Engineering*, 44(5):351–397, 2006.

[51] T. J. Poinsot and S. Lelef. Boundary conditions for direct simulations of compressible viscous flows. *Journal of computational physics*, 101(1):104–129, 1992.

[52] K. Pragati, H. Sharma, et al. Concept of computational fluid dynamics (cfd) and its applications in food processing equipment design. *Journal of Food Processing and Technology*, 3(1), 2012.

[53] K. W. Ragland and K. M. Bryden. *Combustion engineering*. CRC press, 2011.

[54] E. Richardson and E. Mastorakos. Numerical investigation of spark-ignition in a laminar methane-air counterflow. 2005.

[55] V. Robin, A. Mura, M. Champion, O. Degardin, B. Renou, and M. Boukhalfa. Experimental and numerical analysis of stratified turbulent v-shaped flames. *Combustion and flame*, 153(1-2):288–315, 2008.

[56] B. Savard and G. Blanquart. A priori model for the effective lewis numbers in premixed turbulent flames. 2013.

[57] S. K. Scott. *Chemical chaos*. Number 24. Oxford University Press, 1993.

[58] M.-b. Sun, J.-h. Liang, and Z.-g. Wang. Hybrid rans/les simulation of the supersonic flow over two-dimensional cavities. *JOURNAL OF PROPULSION TECHNOLOGY-BEIJING-*, 27(2):119, 2006.

[59] S. R. Turns. An introduction to combustion, concepts and applications mcgraw-hill. *New York*, 1996.

[60] C. S. Yoo, Z. Luo, T. Lu, H. Kim, and J. H. Chen. A dns study of ignition characteristics of a lean iso-octane/air mixture under hcci and saci conditions. *Proceedings of the Combustion Institute*, 34(2):2985–2993, 2013.

[61] H. Zhao. *Advanced direct injection combustion engine technologies and development: diesel engines*, volume 2. Elsevier, 2009.

[62] W. Zuo. Introduction of computational fluid dynamics. *St. Petersburg*, 2005.